Journal of Energy Storage 111 (2025) 115051

Contents lists available at ScienceDirect

Journal of Energy Storage

journal homepage: www.elsevier.com/locate/est

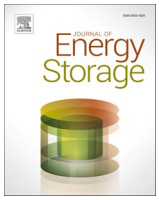

Research Papers

Sizing of energy storage for spinning reserve and efficiency increase in isolated power systems within a data-driven stochastic unit commitment framework

Ayotunde A. Adeyemo [a,*], Francesco Marra [b], Elisabetta Tedeschi [a,c,**]

[a] Department of Electric Energy, Norwegian University of Science and Technology (NTNU), 7034 Trondheim, Norway
[b] Equinor Research Centre, Arkitekt Ebbells veg 10, 7053 Ranheim, Norway
[c] Department of Industrial Engineering, University of Trento, , Via Sommarive, 9, 38123 Povo, Italy

ARTICLE INFO

Keywords:
Stochastic unit commitment
Mixed integer linear programming
Lithium Iron Phosphate Battery
Battery energy storage system
Scenario reduction
Multiple uncertainties

ABSTRACT

This paper proposes a data-driven stochastic unit commitment (SUC) framework for sizing battery energy storage system (BESS) for spinning reserve and efficiency increase in isolated power system. BESS is used to provide spinning reserve to manage the uncertainties in the power system. Additionally, load-shifting demand response (DR) is incorporated in the data-driven SUC model to reduce the size of the BESS required. Also, battery degradation is modelled in the data-driven SUC formulation to make the results as accurate as possible. Furthermore, to reduce the computational burden a novel scenario reduction method based on the Kantorovich distance metric is proposed for selecting scenarios (from the high number of generated scenarios for load and renewable sources) that describe the problem with limited loss of information. The case study is based on an offshore oil and gas platform in the North Sea which has four identical gas turbine generators and is assumed to integrate offshore wind turbines and an offshore solar farm, thus having three sources of uncertainty (load, wind and solar). Five test cases were analyzed: a baseline case without BESS and flexible load (DR), and other cases including degrading BESS and flexible load, either separately or jointly. First, the selected scenarios were analyzed and seen to retain most of the information in the original historical dataset, which validates the accuracy of the proposed scenario reduction method. The results showed that the methodology proposed in this work can be used to get an accurate optimal BESS capacity and that the inclusion of load-shifting DR can help reduce the optimal BESS capacity. Cases where an optimally sized BESS was considered provided cost reductions in the range 2.54 % to 3.68 % and carbon emissions reductions in the range 3.88 % to 4.5 % compared to the baseline case. Finally, the result also showed that battery degradation modelling is important as the cost reduction increased from 2.54 % to 3.68 % when battery degradation is modelled.

1. Introduction

1.1. Motivations

The inherent uncertainty in power systems has consistently posed significant challenges for the operation and control of power grids [1]. Traditionally, this uncertainty was primarily associated with load demand. However, the integration of renewable energy sources (RESs) into power systems has introduced new dimensions of uncertainty in recent years. To ensure the security of supply in such environments, high spinning reserves are typically provided by dispatchable energy sources such as gas turbine generators (GTGs) and coal power plants, which results in increased costs and carbon emissions.

Nomenclature

Sets and indexes	
$t \in T$	Time periods
$k \in GTG$	Gas turbine generator units
$i \in WT$	Wind turbine units
$j \in PV$	Solar photovoltaic units
$l \in BESS$	Battery energy storage system units

(*continued on next page*)

* Corresponding author.
** Correspondence to: E. Tedeschi, Department of Electric Energy, Norwegian University of Science and Technology (NTNU), 7034 Trondheim, Norway.
E-mail addresses: ayotunde.a.adeyemo@ntnu.no (A.A. Adeyemo), elisabetta.tedeschi@ntnu.no (E. Tedeschi).

https://doi.org/10.1016/j.est.2024.115051
Received 10 February 2024; Received in revised form 30 October 2024; Accepted 14 December 2024
Available online 22 January 2025

(*continued*)

$\widetilde{\xi}(\omega) \in \Omega$	Uncertainty space including all scenarios
ω	Index for a scenario
Optimization variables	
π_{ω}	Scenario probability
Uncertainty modelling	
$\widetilde{\xi}$	Sampled stochastic process
p	Index for stochastic variable that can be load (l), wind speed (w), or solar irradiation (pv)
$\widehat{F}^{p}_{h,t}(\widetilde{\xi}^{p}_{t})$	Marginal empirical cumulative distribution function for load, wind speed or solar irradiation
$F^{p}(\widetilde{\xi}^{p})$	Multivariate joint distribution for load, wind speed or solar irradiation

Energy storage systems (ESSs), acknowledged as vital components of future power systems [2,3], offer a promising solution. ESSs can provide spinning reserves and enhance efficiency, leading to cost reductions and lower carbon emissions while ensuring reliable system operation. The importance of ESS is even more pronounced in small-scale isolated power systems, where load demand is highly volatile, and the uncertainty from RESs is significant due to the limited number of generation points. In contrast, larger power systems benefit from distributed renewable sources, which aggregate to reduce overall uncertainty.

According to the International Energy Agency, the global installed capacity of grid-scale battery energy storage systems (BESS) reached 28 GW in 2022, with 11 GW added in 2022 alone [4]. The rapidly declining cost of batteries [5] is expected to further drive the adoption of BESS to address the numerous challenges faced by modern power systems. However, determining the optimal size of ESS for providing spinning reserves and increasing efficiency is a complex task due to the multiple sources of uncertainty inherent in systems with significant renewable energy integration.

1.2. Literature review

The simplest way to solve the storage sizing problem is by formulating a deterministic unit commitment (DUC) problem. The main benefit of the DUC is its low computational burden. The uncertainty in the load and renewable sources can be dealt with by allocating a large spinning reserve margin. However, the DUC does not guarantee a high energy security and in some cases may lead to higher operational cost. For example, DUC was solved in [6] and in all the evaluated cases it had a higher cost than the corresponding stochastic unit commitment (SUC) approach, while also having load shedding which implies reduced security of power supply. Due to the high cost and limited reliability of the traditional DUC some authors have proposed alternative unit commitment (UC) formulations that yield a performance close to that of a SUC at a reasonably low computational burden. These UC formulations include interval unit commitment [7], improved interval unit commitment (IIUC) [8], DUC with probabilistic reserve constraint [9], chanced constrained UC [10], robust UC [11] and hybrid methods [12]. The IIUC proposed in [8] was used to solve the scheduling of dispatchable generation and pumped hydro energy storage (PHES) in the Belgian power system. The IIUC formulation models the hydraulic constraints of the PHES when the PHES is providing regulation services. The IIUC model has three forecast scenarios and four ramping scenarios. All the scenarios in a SUC are reduced to the three forecast scenarios in the IIUC. The three forecast scenarios include the central forecast scenario, the upper bound scenario, and the lower bound scenario. The goal of the IIUC is to reduce the computational cost of the UC while achieving a cost-efficient schedule. Bruninx et al. [9] proposed a DUC formulation with probabilistic reserve constraints. They defined distinct reserve levels based on the probability distribution of wind forecast error i.e., the probability distribution of wind forecast error is divided into L regions with each region representing a reserve level and having a certain probability. The reserve activation cost depends on the probability of activation of the reserve level. However, the quality of the solution obtained with this method depends on the knowledge of the probability of activation of each power plant offering reserve, otherwise a wrong estimate of the activation probability may impact the accuracy of the result. The authors in [13] proposed an energy storage (ES) sizing approach by solving a chance-constrained optimization (CCO) with correlated uncertainties. The goal in the paper was to minimize the total cost by optimizing the size of the ES, thermal units generation power, wind curtailment and load shedding. The model in the paper considered correlation of the forecast errors of wind farm and load at different buses. However, they assumed a parametric distribution for the load and wind which is not always a realistic assumption, particularly in isolated power systems. The main benefits of these alternative approaches are that they allow the modelling of a bit of stochastic formulation while having low computational burden. Nevertheless, these alternative approaches may not necessarily be the best methods for solving the UC problem used for sizing the ES especially when used in isolated power grids. We believe a good way to deal with uncertainty in power systems is through the use of SUC formulation. Also, the focus on isolated power systems allows a reduced computational burden compared to interconnected power systems with a high number of buses, particularly in the case of SUC formulation.

In this paper, energy storage sizing using a data-driven SUC model with battery degradation and flexible load (demand response (DR)) is proposed. Many papers in literature, including the works in [14–23] have proposed SUC models but most of these works assume a parametric distribution for the uncertainties, which is not always valid. The underlying factor in the SUC model is how the scenarios are generated. Scenario generation can either use parametric or non-parametric distribution. SUC models with scenario generation that uses non-parametric distribution are referred to as data-driven SUC models as the distribution is inferred from historical data of the source of uncertainty. One problem with many SUC formulations is that a parametric distribution is assumed for the RESs (such as wind power) and the load demand. The empirical data for the wind speed does not usually follow a probability distribution [8] as assumed in some studies ([13,24]). For some isolated power systems, such as the offshore oil and gas platform (OOGP) in this work, the load demand does not usually follow a particular probability distribution, either. However, data-based methods have demonstrated the ability to adequately describe more complex patterns in historical datasets [25]. Thus, it is important to use good data-driven scenario generation and scenario reduction methods. Some works have studied data-driven SUC. The authors in [26] proposed a data-driven SUC scheme with DR for managing the uncertainty in load demand and wind power. DR is used to increase the flexible ramping capability of the thermal generators to avoid load shedding and wind curtailment. However, this study does not consider ESS for providing flexible ramping capability. The authors in [1] also used a data-driven scenario generation approach in a stochastic programming formulation for sizing of ES in an isolated power system but only considered two sources of uncertainty and did not model battery degradation nor include DR. The works in [26–34] have also studied data-driven SUC but none of these works considered battery degradation and DR.

BESS inclusion in the UC offers flexibility and ability to manage the uncertainty in the load and renewable energy generation. However, the modelling of the cost of the BESS needs to consider the degradation of the BESS for an accurate cost estimate. Very few works have modelled BESS degradation in the UC model. The authors in [35,36] proposed a particle swarm optimizer to solve the UC of a micro-grid while considering battery degradation. However, in both studies the battery degradation does not consider calendar aging and the cost of the battery is not considered in the total system cost to see if there is benefit in using BESS. The authors in [37] proposed a SUC in a micro-grid while considering battery degradation. Benders decomposition was used to minimize the BESS cycle aging and life cycle cost. Unlike the works in [35,36], the

work in [37] includes the BESS cost (life cycle cost) in the total system cost. However, like the works in [35,36], the calendar aging was not considered in the battery degradation. The authors in [38] proposed a novel matrix representing BESS energy capacity degradation which is used in stochastic optimal planning of BESS for micro-grids including solar and wind generation. The parameters optimized are the BESS size and installation year of BESS. However, the BESS capacity matrix uses a simple degradation model and does not use depth of discharge (cycle counting) and temperature in a comprehensive model. Also, cycle aging and calendar aging are not separately modelled.

While BESS offers flexibility and can help manage the uncertainty in the load and RESs, the high cost of ES makes its integration less appealing especially when the ES capacity required is large. As a result of this, some works have studied the use of DR for providing flexibility and managing uncertainties in the power system. Some studies have used DR alone [26] while others have used it to reduce the size of the ES required [39]. The authors in [24] used particle swarm optimization method to optimize the cost of energy consumption of a grid-connected micro-grid with renewable energy sources, ESS and DR programmes. The DR programmes help to improve the voltage profile and reduce cost. The authors in [39] proposed to use DR to meet the transmission constraints in the UC of a smart grid with solar photovoltaic (PV) panels, wind turbines (WTs), thermal generation units, smart houses and BESS. Tabu search was used to determine the optimal schedule of operation of the thermal generation units, BESS and the controllable loads in the smart houses. The use of DR in the proposed smart grid reduced the size of the BESS. The benefit of the smart grid was increased when DR was considered. The authors in [40] proposed a mixed-integer programming approach for UC of a micro-grid with BESS and incentive-based DR. The BESS and DR are used to manage the uncertainty in load and RES. The use of BESS and DR reduces the system cost compared to the case without BESS and DR. DR was also used in a new SUC of a nine-unit test system with wind power and ESS [41]. The SUC formulation was used to determine the optimal ESS size while considering DR. The use of ESS and DR helps reduce the system cost while the ESS helps increase wind power utilization. Finally, DR was used in two operation stages in [26]: in the day-ahead stage, load-shifting DR reduces the ramping requirements by changing the load profile; in the real-time stage, reserve-capacity DR enables the ramping capability by providing reserve for the rebalance of wind power variation. The type of DR used in this work is similar to the load-shifting DR. It should be noted that as opposed to the DR implemented in these papers, the DR considered in this work comes at no cost since this is an isolated power system and the system operator can modify the operation of the flexible load for free. The water injection system (WIS) in OOGPs is considered as the flexible load in this work.

1.3. Opportunities and challenges

This work presents significant opportunities for enhancing power supply security and efficiency by optimizing the size of the BESS using a robust sizing methodology that integrates data-driven approaches to account for uncertainty in load and RESs. BESS can quickly respond to fluctuations in power demand and supply, thus providing a reliable source of spinning reserve that can stabilize the grid during unexpected outages or sudden changes in load, thus increasing the security of power supply. The study in this paper also highlights the opportunity for BESS to improve overall system efficiency. By optimally sizing the BESS, the power system can minimize the need to operate more generators solely for reserve purposes and decrease the need for inefficient part-load operation of generators. This leads to a more efficient use of energy resources and a reduction in fuel consumption and emissions. This paper also identifies the potential for cost savings through the integration of BESS. Properly sized storage can reduce the operational costs associated with maintaining spinning reserves. The use of data-driven approaches for sizing further enhances the precision of these estimates, leading to more accurate investment decisions. Additionally, integrating optimally sized BESS allows for better integration of RESs, reducing the reliance on fossil fuels and consequently lowering greenhouse gas emissions. This paper's use of a data-driven stochastic unit commitment framework presents an opportunity to leverage large datasets and advanced analytics in the decision-making process. This approach enables more accurate and robust sizing of ESS by accounting for uncertainties and variabilities in load demand and renewable energy generation, leading to more resilient and adaptable power systems. Finally, the findings from this research have broader implications beyond isolated power systems. The methodologies and insights gained can be applied to other sectors, such as microgrids, remote communities, and critical infrastructure, where reliable and efficient energy supply is paramount.

However, there are also challenges associated with the study in this paper. One of the primary challenges is the complexity involved in stochastic modelling and the computational demands of solving the UC problem within this framework. The need to consider multiple uncertainties, such as load fluctuations and renewable energy variability, makes the modelling process intricate and resource-intensive. This complexity can be a barrier to practical application, especially in systems with limited computational resources. However, unlike for large interconnected grids, it is expected that the complexity and computational burden should be manageable for most isolated power systems of reasonable size. The effectiveness of a data-driven approach heavily relies on the availability and quality of data. In isolated power systems, particularly in remote or underdeveloped regions, obtaining accurate and comprehensive datasets can be challenging. Inadequate data can lead to suboptimal BESS sizing, reducing the potential benefits of the system. While the research in this paper provides valuable insights for the specific context of isolated power systems, there may be challenges in scaling and generalizing the findings to different types of power systems or to larger scales. The unique characteristics of each power system, such as its load profile, generation mix, and geographic location, mean that the optimal sizing of BESS might vary significantly, requiring special care when exporting the research approaches and results to other contexts.

1.4. Contributions and paper organization

Out of all the contributions available in the literature that were analyzed, only 34 % considered both stochastic modelling and data-driven modelling of sources of uncertainty in the UC formulation. Moreover, only 12.5 % considered the effect of battery degradation in UC formulation and only 22 % included DR as a potential flexibility tool in UC formulation. None of the papers considered both battery degradation and DR at the same time. It is of utmost importance to consider both battery degradation and DR concomitantly as this allows us to see how DR can be effectively utilized to reduce battery degradation and reduce cost. Furthermore, there is no single work among all the ones reviewed that has used a SUC model that incorporates three sources of uncertainty (in our case load, wind speed and solar irradiation), data-driven modelling of the sources of uncertainty, battery degradation and DR. Also, the quality of scenario reduction method determines how statistically stable the BESS sizing is. Not many studies in literature have been able to reduce the number of scenarios without significant loss of information in the original data. To solve this problem, the work in [1] proposed a scenario reduction method. This work goes one step further by improving the scenario reduction method proposed in [1] in a novel way. Thus, the main contributions of this work are:

- A novel scenario reduction method is proposed.
- An effective DR strategy for reducing BESS size and battery degradation cost is included.
- Data-driven SUC modelling that incorporates three sources of uncertainty, accurate battery degradation and flexible load (DR) is proposed.

The novel modification to the scenario reduction method proposed in [1] is explained in section 4.2. Table 1 shows the summary of the literature review and highlights the advantages produced by the proposed approach.

This paper is structured as follows:

Section 2 describes the methodology for the BESS sizing in this work. Section 3 describes the stochastic unit commitment model including the battery degradation model and smart load management model. In section 4, the scenario generation and reduction models are described. Section 5 explains the simple algorithm for the determination of the optimal BESS capacity while section 6 describes the case study. Finally, section 7 presents the results and discussion.

2. Methodology for BESS sizing in an isolated power system

The methodology for BESS sizing includes a few steps and is depicted in the flow chart of Fig. 1. In Step 1, 1000 profiles for each uncertainty (load, wind speed, and solar irradiance) are generated based on historical datasets, reflecting a broad range of possible conditions. In Step 2, these profiles are ranked using the Kantorovich distance, which measures similarity between distributions, allowing for a representative selection. These ranked profiles are then joined together to form scenarios via a novel method detailed in Section 4.2, ensuring realistic time-correlated scenarios as input into the optimization framework.

In step 3, the 1000 scenarios are mapped into a Q-dimensional space where Q is the number of uncertainties. Scenario reduction is then performed to select 50 scenarios using k-means. In step 4, the selected scenarios are then incorporated into the SUC model in section 3 and the optimal BESS size in each test case defined in Table 8 is determined using the algorithm in Fig. 2. Sensitivity analysis is then performed in step 5 to quantify the reduction in total UC cost at the optimal BESS capacity in each test case with BESS as the BESS capacity cost reduces and the change in the optimal BESS size at higher renewable penetration. In step 6, the test case with battery degradation modelling and flexible load is selected and the optimal BESS capacity in this test case is used, as this test case is the most reasonable. Also, reduction in total UC cost in this test case with respect to the other test cases is evaluated using the results in step 4 and 5.

3. Stochastic unit commitment model

The SUC model is used to determine, a day-ahead, the optimal schedule of the dispatchable generation units to meet the load while considering the uncertainty in the load and RESs.

3.1. Objective function

The objective of the SUC is to minimize the total cost for a day (i.e. daily UC) while maintaining a high security of the power supply. The objective function for the SUC problem is given in Eq. (1).

$$TUCC = min\left\{ \sum_{k\in GTG}\sum_{t} \overbrace{\left(u_k SU_{k,t}\right)}^{1} + \overbrace{c_{co2} d_k SU_{k,t}}^{2} \right.$$
$$+\pi_w \sum_{\omega\in\Omega}\left(\sum_{k\in GTG}\sum_{t} \overbrace{\left(c_{ng} U_{k,t}\left(a_k {P_{k,t}}^2 + b_k P_{k,t} + c_k\right)\right.}^{3} \right. \tag{1}$$
$$\left.\left. \underbrace{+c_{co2} U_{k,t}\left(x_k {P_{k,t}}^2 + y_k P_{k,t} + z_k\right)}_{4} \right) + \underbrace{BESS_{degcost}}_{5} \right\}$$

Table 1
Summary of literature survey.

Ref.	Stochastic	Data-driven	Sources of uncertainty			BESS degradation	Demand response
			Load	Wind	Solar		
[1]	✓	✓	✓	✓	×	×	×
[6]	✓	×	✓	✓	×	×	×
[8]	×	×	×	✓	×	×	×
[9]	×	×	×	✓	×	×	×
[13]	×	×	✓	✓	×	×	×
[14]	✓	×	×	✓	×	×	✓
[15]	✓	×	×	✓	✓	×	✓
[16]	✓	×	×	✓	×	×	×
[17]	✓	×	×	×	✓	×	×
[18]	✓	×	✓	×	×	×	×
[19]	✓	✓	✓	✓	×	×	×
[20]	✓	×	×	✓	✓	×	×
[21]	✓	×	×	✓	✓	×	×
[22]	✓	×	✓	✓	✓	×	×
[23]	✓	×	×	✓	×	×	×
[24]	✓	×	✓	✓	✓	×	✓
[26]	✓	✓	✓	✓	×	×	✓
[27]	✓	✓	×	✓	✓	×	×
[28]	✓	✓	×	✓	×	×	×
[29]	✓	✓	×	×	×	×	×
[30]	✓	✓	×	✓	×	×	×
[31]	✓	✓	×	✓	×	×	×
[32]	✓	✓	×	✓	×	×	×
[33]	✓	✓	✓	×	×	×	×
[34]	✓	✓	×	✓	×	×	×
[35]	×	×	✓	×	×	✓	×
[36]	×	×	✓	×	×	✓	×
[37]	✓	×	✓	✓	✓	✓	×
[38]	✓	×	✓	✓	✓	✓	×
[39]	×	×	×	×	✓	×	✓
[40]	×	×	✓	✓	✓	×	✓
[41]	✓	×	×	✓	×	×	✓
This paper	✓	✓	✓	✓	✓	✓	✓

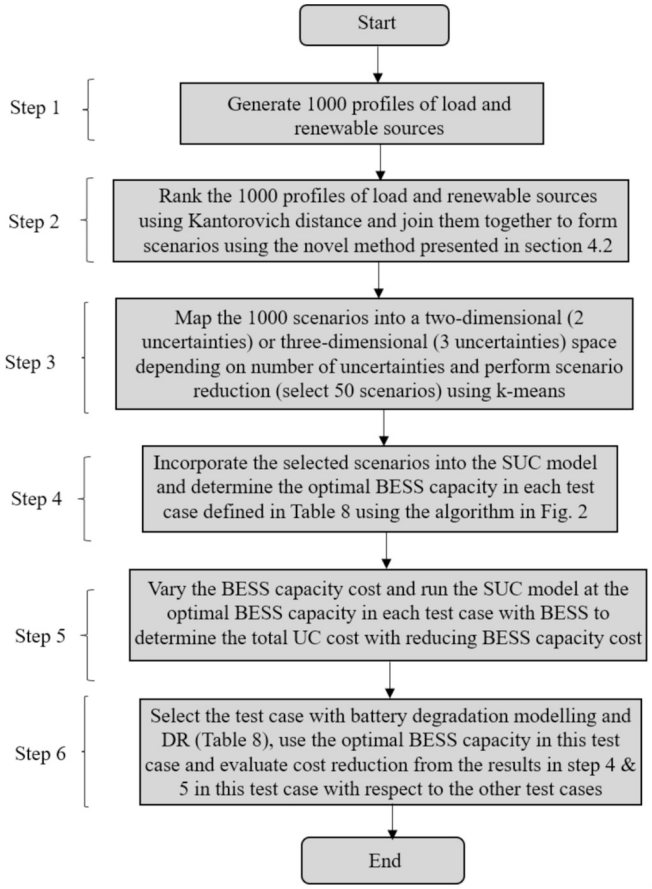

Fig. 1. Flow chart of the methodology for BESS sizing for spinning reserve in an isolated power system using data-driven SUC.

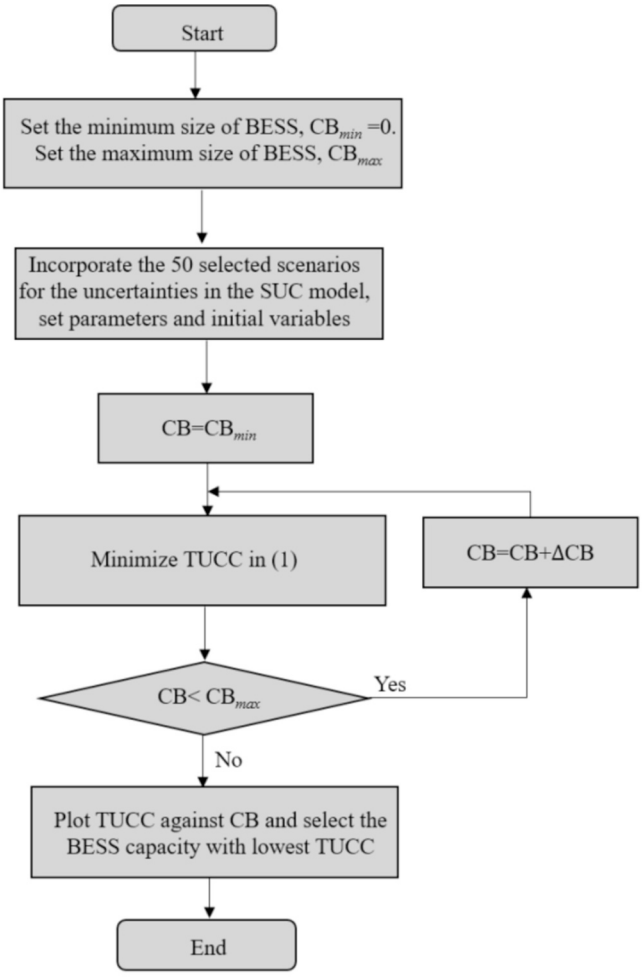

Fig. 2. Flow chart of the BESS sizing algorithm.

where *TUCC* is the total unit commitment cost (TUCC), k is the index for GTG, t is the index for time period, u_k is the start-up cost of the kth unit, c_{co2} is the carbon emission tax in $\frac{\$}{kg_{co2}}$, d_k is the carbon emissions per start-up, $SU_{k,t}$ is the start-up status of the kth unit at hour t, π_ω is the scenario probability, ω is the index for scenario, Ω is the set of all scenarios, c_{ng} is the cost of natural gas in $\frac{\$}{Sm^3}$, $U_{k,t}$ is the on/off status of the k-th unit at hour t ($U_{k,t}$ is 1 when the k-th GTG is running and is 0 when the k-th GTG is off), a_k, b_k and c_k are the fuel consumption coefficients, x_k, y_k and z_k are the carbon emission coefficients, $P_{k,t}$ is the power generated by the kth unit at hour t and $BESS_{degcost}$ is the battery degradation cost.

In Eq. (1), the terms are labeled 1–5. The GTGs take some time to start-up before they can be loaded. During this time a significant amount of fuel is burned which leads to fuel cost and greenhouse gas emissions which lead to emissions tax. The start-up fuel cost and start-up emission tax are expressed in Eq. (1) in the first and second term respectively. The third term is the production fuel cost (i.e. the fuel cost when the GTGs are running), the fourth term is the production emission tax (i.e. emission tax when the GTGs are running) and the fifth term is the BESS degradation cost. Eq. (1) expresses a detailed plan for which GTGs should be used, when to turn them on or off and how to do this in the most efficient and cost-effective way to meet the load demand without loss of power.

Note that the fuel cost of the GTGs is a quadratic function. To make the problem solvable using mixed integer linear programming (MILP), the GTG cost function is piecewise linearized. In this paper, 4 linear segments are used for the GTG cost function. Note that the UC schedule in Eq. (1) is the same for all scenarios, thus, the first and second term in Eq. (1) are separated from the third, fourth and fifth term because the start-up fuel cost and start-up emission tax will be the same for all scenarios. Note that the BESS degradation cost will be different for each scenario which explains why it is grouped with the third and fourth terms and multiplied by the scenario probability, π_ω.

Note that this study only considers the sizing of the BESS and not how the BESS is operated. In the BESS sizing in this study, the operation of the BESS is optimized in the hours timescale while operational optimization will typically optimize the operation of the BESS in the minutes timescale. The datasets used in this work are hourly datasets.

3.2. Constraints

However, Eq. (1) is subject to some constraints i.e. we seek a solution with the minimum TUCC among all the solutions that satisfy all the constraints. The constraints that must be satisfied while minimizing the TUCC in Eq. (1) are listed below.

3.2.1. Power generation limits

The power generation of each GTG must be limited between the minimum and maximum generation levels.

$$P_k^{min} \leq P_{k,t} \leq P_k^{max}, \forall t \tag{2}$$

where P_k^{min} is the minimum power generation for the k-th unit, P_k^{max} is the maximum power generation for the k-th unit.

3.2.2. Power balance

The sum of the powers generated by the GTGs, WTs, solar PV panels and BESS must be equal to the load demand.

$$P_t^d + P_{wis,t} + P_{hvac} = \sum_{k \in GTG} P_{k,t} + \sum_{i \in WT} P_{i,t} + \sum_{j \in PV} P_{j,t} + \sum_{l \in BESS} P_{l,t} - P_{dump,t}, \forall t \quad (3)$$

where P_t^d is the power demanded by the load without the WIS load in time t, $P_{wis,t}$ is the WIS load in time t, P_{hvac} is the power consumed by the BESS heating, ventilation and air-conditioning, i is the index for WT, j is the index for solar PV, l is the index for BESS, $P_{l,t}$ is the power supplied or absorbed by the l-th BESS in time t, $P_{l,t}$ is positive for discharging and negative for charging, and $P_{dump,t}$ is the dump load in time t.

Note that the dump load, $P_{dump,t}$, in Eq. (3) is for dissipating the excess power when the load minus the power from RESs is less than the minimum generation of the GTGs. In other words, the dump load allows the GTGs to always operate above the minimum generation level, even in scenarios where the load is low and the renewable power is high.

3.2.3. Minimum up time

Dispatchable generation units usually have a minimum up time. This is the minimum period the generator must be running after it is started before it can be turned off. This is given as follows:

$$tup \bullet SU_{k,t} - \sum_{h=0}^{tup-1} U_{k,t+h} \leq 0, \forall k, \forall t \quad (4)$$

$$tup = \begin{cases} MUT \text{ if } 24 - (t-1) \geq MUT \\ 24 - (t-1) \text{ if } 24 - (t-1) < MUT \end{cases}$$

where MUT is the minimum up time (hours).

3.2.4. Minimum down time

Dispatchable generation units usually also have a minimum down time. This is the minimum period the generator must remain off after it is turned off before it can be turned on. This is given as follows:

$$SU_{k,t} + \sum_{h=1}^{tdown} U_{k,t-h} \leq 1, \forall k, \forall t \quad (5)$$

$$tdown = \begin{cases} MDT \text{ if } t > MDT \\ t - 1 \text{ if } t \leq MDT \end{cases}$$

where MDT is the minimum down time (hours).

3.2.5. Ramp up limit

The ramp up limit is the maximum rate at which the power of a GTG can be increased, which can typically be in MW/h. The ramp up limit must be satisfied at all hours.

$$P_{k,t} - P_{k,t-1} \leq ramp_k^{up}, \forall t \quad (6)$$

where $ramp_k^{up}$ is the ramp up limit of k-th GTG.

3.2.6. Ramp down limit

The ramp down limit is the maximum rate at which the power of a GTG can be decreased, which can typically be in MW/h. The ramp down limit must be satisfied at all hours.

$$P_{k,t-1} - P_{k,t} \leq ramp_k^{down}, \forall t \quad (7)$$

where $ramp_k^{down}$ is the ramp down limit of k-th GTG.

3.2.7. Spinning reserve and downward reserve constraints

The spinning reserve is the amount of power available in a running generation unit that can be utilized to meet sudden load demand increase. The downward reserve is the amount of power that can be decreased following a sudden load decrease i.e., the amount of power above minimum generation level. Given that the SUC model considers all the potential scenarios that could occur, the spinning reserve constraint and downward reserve constraint are implicitly satisfied.

3.2.8. Battery energy storage system constraints

The BESS must satisfy some constraints. The power generation constraint is given in Eq. (8).

$$P_l^{max\_c} \leq P_{l,t} \leq P_l^{max\_d}, \forall t \quad (8)$$

where $P_l^{max\_d}$ is the maximum discharge power of the l-th BESS, $P_l^{max\_c}$ is the maximum charge power of the l-th BESS.

Note that $P_l^{max\_c}$ is negative. Note that in this work, the charging and discharging efficiencies are lumped together to a roundtrip efficiency for simplicity and this is used in only the charging phase. Thus, the BESS power is given as:

$$P_{l,t} = u_l \bullet P_{l,t}^d + (1 - u_l) \bullet \frac{P_{l,t}^c}{BESS_{rt\_eff}} \quad (9)$$

where $BESS_{rt\_eff}$ is the BESS roundtrip efficiency, $P_{l,t}^d$ is the BESS discharging power and $P_{l,t}^c$ is the BESS charging power, u_l is the status of the BESS which is 1 for discharging and 0 for charging.

Let $SOC_{l,t}$ be the state of charge (SOC) of the l-th BESS. $SOC_{l,t}$ must be maintained within a certain range in order to prolong the life of the BESS. The constraint is given as follows:

$$SOC_l^{min} \leq SOC_{l,t} \leq SOC_l^{max} \quad (10)$$

where SOC_l^{min} is the minimum SOC of the l-th BESS unit and SOC_l^{max} is the maximum SOC of the l-th BESS unit.

The change in the SOC from one time step to the next is given as follows:

$$SOC_{l,t} = \begin{cases} SOC_{l,t-1} - \frac{P_{l,t}\Delta t}{BESS_{cap}} \text{ if } P_{l,t} \geq 0 \\ SOC_{l,t-1} - \frac{P_{l,t}\Delta t BESS_{rt\_eff}}{BESS_{cap}} \text{ if } P_{l,t} < 0 \end{cases} \quad (11)$$

where $BESS_{cap}$ is the nominal capacity of the BESS in MWh.

To ensure a fair usage of the BESS, the initial and final SOC on the UC day are made equal as in Eq. (12)

$$SOC_{ini} = SOC_{fin} \quad (12)$$

where SOC_{ini} is the BESS SOC at the start of the day and SOC_{fin} is the BESS SOC at the end of the day. The initial SOC (SOC_{ini}) in this work is given in Table A2 in appendix A.

3.2.9. Smart load management of flexible load

Smart load management of flexible load refers to shifting of the power consumption of a flexible load to other hours otherwise known as "load-shifting DR" [26]. In this scheme the average power consumption of the flexible load is maintained but the profile of the flexible load can be modified. Flexible loads are loads that can be controlled in a smart way (load-shifting DR) to reduce the TUCC and increase the efficiency of the thermal power plants in a power system. In an OOGP WISs are an example of flexible load. With flexible loads it is possible to decrease the power consumption when the load demand is high, or the renewable generation is low and increase the power consumption when the load demand is low or renewable generation is high. In the case study of this work (which is described in section 6) the flexible load is a WIS. It is not very critical to always run the WIS at high power as what is required is that a certain volume of water should be injected in the oil well over the useful life of the oil platform. In this work it is assumed that an average of 50 % of the rated capacity of the WIS is consumed by the WIS in a typical day. Thus, the WIS load can be increased in some hours and decreased in some other hours. What is important is that the average power consumption is equal to a defined fig. (50 % rated capacity in the considered case, but it can be arbitrarily modified). The WIS constraints are given in Eqs. (13)–(14).

$$\sum_{t=1}^{24} P_{wis,t} = 0.5 \bullet P_{wis}^{n} \bullet 24 \tag{13}$$

$$0 \le P_{wis,t} \le P_{wis}^{n} \tag{14}$$

where $P_{wis,t}$ is the WIS power at hour t, P_{wis}^{n} is the rated power of the WIS.

3.3. Power generation using renewable energy sources

3.3.1. Power generation from wind turbines

The power generation from each WT is given by Eq. (15).

$$P_{i,t} = \begin{cases} 0 \text{ if } \xi_t^w(\omega) < w_{ci} \\ P_w^n \left(\dfrac{\xi_t^w(\omega)}{w_n}\right)^3 \text{ if } w_{ci} \le \xi_t^w(\omega) < w_n \\ P_w^n \text{ if } w_n \le \xi_t^w(\omega) < w_{co} \\ 0 \text{ if } w_{co} \le \xi_t^w(\omega) \end{cases} \tag{15}$$

where $\xi_t^w(\omega)$ is the wind speed at time t in scenario ω, P_w^n is the rated power of each WT, w_{ci} is the cut-in wind speed, w_n is the rated wind speed, w_{co} is the cut-off wind speed.

The parameters of the considered WTs are given in Table A3 in Appendix A.

3.3.2. Power generation from solar photovoltaic panels

The power generation from a solar PV panel is given in Eq. (16) [42].

$$P_{j,t} = P_{pv}^{n} \bullet \left(\frac{\xi_t^{pv}(\omega)}{R_{ref}}\right) \bullet \left(1 + k_{temp}\left(T_{cell} - T_{ref}\right)\right) \bullet MPPT_{eff} \bullet AC_{eff} \tag{16}$$

$$T_{cell} = T_{air} + \left(\frac{NOCT - 20}{800}\right) \bullet \xi_t^{pv}(\omega) \tag{17}$$

where, P_{pv}^{n} is the rated power of each solar PV panel, $\xi_t^{pv}(\omega)$ is the solar irradiation at time t in scenario ω, R_{ref} is the solar irradiation at reference conditions and is usually 1000 W/m^2, k_{temp} is the power temperature coefficient of the solar PV panel, T_{cell} is the actual cell temperature, T_{ref} is the cell temperature at reference conditions, $MPPT_{eff}$ is the maximum power point tracking converter efficiency, AC_{eff} is the DC-AC inverter efficiency, T_{air} is the ambient air temperature, $NOCT$ is the nominal operating cell temperature.

The parameters of the considered solar PV panels are given in Table A3 in Appendix A.

3.4. BESS degradation model

Lithium iron phosphate (LFP) is used in this work as BESS. The capacity loss for a LFP battery is given in Eqs. (18)–(21) [43].

$$C_{loss}[\%] = C_{cyc_{LFP}} + C_{cal_{LFP}} \tag{18}$$

$$C_{cal_{LFP}} = \alpha_{cal_{LFP}} \bullet e^{\beta_{cal_{LFP}} \bullet T_{cont}} \bullet \frac{t_d}{30}^{0.5} \tag{19}$$

$$C_{cyc_{LFP}} = \alpha_{cyc_{LFP}} \bullet e^{\beta_{cyc_{LFP}} \bullet T_{cont}} \bullet NC^{0.5} \tag{20}$$

$$NC = t_d \bullet c_d \tag{21}$$

where t_d is the number of days till the end of life (EOL) and c_d is the number of cycles demanded by the model for a typical day, T_{cont} is temperature in K. $\alpha_{cal_{LFP}}$ and $\beta_{cal_{LFP}}$ are the coefficients for calendar aging. α_{cyc_LFP} and $\beta_{cyc_{LFP}}$ are the coefficients for cycling aging. The values for α_{cal_LFP}, $\beta_{cal_{LFP}}$, α_{cyc_LFP} and $\beta_{cyc_{LFP}}$ are gotten from [43] for a BYD LFP battery.

In order to determine the cost, the total number of days till end of life needs to be determined. By choosing C_{loss} to be equal to EOL capacity loss, substituting (19)–(21) in (18) and rearranging the result, we have:

$$t_d = \frac{100 - EOL}{\left(\alpha_{cyc\_LFP} \bullet e^{\beta_{cyc_{LFP}} \bullet T_{cont}} \bullet c_d^{0.5} + \alpha_{cal\_LFP} \bullet e^{\beta_{cal_{LFP}} \bullet T_{cont}} \bullet \frac{1}{30}^{0.5}\right)^2} \tag{22}$$

$$BESS_{degcost}[\$] = \frac{1}{t_d} \bullet BESS_{cap\_c} \tag{23}$$

$$BESS_{cap\_c} = 1000 \bullet BESS_{cap} \bullet BESS_{cap\_kwh} \tag{24}$$

where EOL is the end-of-life capacity in %, $BESS_{cap\_c}$ is the capital cost of the BESS, and $BESS_{cap\_kwh}$ is the BESS cost per kWh. All the parameters used for the battery degradation modelling are given in table A2 in Appendix A.

Note that the equation in (22) is not linear. The equation was piecewise linearized so that the battery degradation model can be used in the SUC to be solved with a MILP. In this paper, 48 linear segments were used in the piecewise linearization of the battery degradation cost.

4. Scenario generation and scenario reduction methodology

The ideal way to solve the BESS sizing problem involves using a large number of scenarios. However, this may make the problem computationally intractable. It is therefore necessary to reduce the number of scenarios. Thus, the main objective is to select a number of opportune scenarios that, when used, give a solution that is statistically close to the solution of the problem. This requires selecting scenarios that are distributed in the uncertainty space in a way that represents the statistical properties of the potential scenarios that the power system may encounter. Thus, the different possible scenarios that the power system may encounter in a typical day are generated and used for the BESS sizing problem.

In order to accurately represent the uncertainties, the generated scenarios must reproduce the cyclostationarity of the historical data. To ensure this, we consider using a dataset composed of one-year long hourly time series for load, wind speed and solar irradiation.

Given that this paper considers a data-driven scenario generation, the marginal distribution is inferred from the historical data. In addition, the marginal distribution is inferred first, before inferring the joint distribution. Since we do not consider parametric distribution for the considered uncertainties (load, wind speed and solar irradiation), a kernel density estimation (KDE) method is used to infer the marginal distributions. The KDE computes a non-parametric smooth representation of the marginal distributions of load, wind speed and solar irradiation as

$$\widehat{F}_t^p\left(\xi_t^p\right) = \frac{1}{n}\sum_{i=1}^{n} \int_{-\infty}^{\xi_t^p} K_h\left(r - \widetilde{\xi}_i^p\right) dr \tag{25}$$

where $\widehat{F}_t^p$ is the cumulative distribution function and $\widehat{F}_t^p\left(\xi_t^p\right)$ represent the cumulative probability up to the point $\widetilde{\xi}_t^p$, $\widetilde{\xi}_t^p$ is the value of a stochastic variable in a random scenario at time t and p can be pv (PV), w (WT) or l (load), ξ_i^p is an observed data point for the stochastic variable where p is as defined in ξ_t^p, n is the size of the dataset used for scenario generation which is 365 in this paper and $K_h\left(r - \widetilde{\xi}_i^p\right)$ is the kernel function. In this work, a gaussian kernel is used. The gaussian kernel is written in Eq. (26) and the overall cdf equation is written in Eq. (27).

$$K_h\left(r - \widetilde{\xi}_i^p\right) = \frac{1}{\sqrt{2\pi}h_p} exp\left(-\frac{\left(r - \widetilde{\xi}_i^p\right)^2}{2{h_p}^2}\right) \tag{26}$$

$$\widehat{F}_t^p\left(\widetilde{\xi}_t^p\right) = \frac{1}{n}\sum_{i=1}^{n}\int_{-\infty}^{\widetilde{\xi}_t^p}\frac{1}{\sqrt{2\pi}h_p}exp\left(-\frac{\left(r-\widetilde{\xi}_i^p\right)^2}{2{h_p}^2}\right)dr \tag{27}$$

where h_p is the bandwidth of the KDE.

To represent the statistical correlation of the load, wind speed or solar irradiation along its temporal dimension, we propose to use a copula-based approach. In other words, we express the joint distribution of the load, wind speed or solar irradiation vector as a suitable combination of the marginals at the various times t and a copula function for $p = \{l, w, pv\}$, so that the joint distribution becomes in line with Sklar's theorem,

$$F^p(\widetilde{\xi}^p) = C^p\left(\widehat{F}_{h,1}^p(\widetilde{\xi}_1^p), \ldots, \widehat{F}_{h,T}^p(\widetilde{\xi}_T^p)\right) \tag{28}$$

where $F^p(\widetilde{\xi}^p)$ is the joint distribution for the load, wind or solar vector, $\widetilde{\xi}^p$ is a randomly sampled scenario for load, wind or solar, $\widehat{F}_{h,1}^p(\widetilde{\xi}_1^p), \ldots, \widehat{F}_{h,T}^p(\widetilde{\xi}_T^p)$ are the marginal empirical cumulative distribution functions at time $t = 1, \ldots, T$.

In this work, we propose to use a Gaussian copula as it is reported to be able to model temporal dependencies [44]. We then propose to use copula-based approaches to generate scenarios from F^p. There are five steps in this approach:

1. Generate the cdf of the marginals using Eq. (27)
2. Compute the correlation, *rho*, between the cdf of the marginals in step 1
3. Generate random samples of a standard multivariate normal distribution (z$\sim N(0,1)$) using the correlation, *rho*
4. Compute the cdf of samples generated in step 3 to make the samples uniform over [0,1] $u_t^p = \Phi(z)$
5. Compute the inverse cdf transformation of the result in step 4 $\widetilde{\xi}_t^p = \widehat{F}_t^{p-1}(u_t^p)$

These five steps are implemented in Matlab, but before the five steps it is necessary to group the data in case it is not grouped. If the data is a one-year long or more than one-year, group the data hour by hour. For example, a one-year long data should be 24 by 365, and a 180-day data should be 24 by 180. After the data is grouped, the five steps described above can be applied. The pseudocode for the five steps in Matlab is given below:

1. Initialize the variable to contain the marginals to zeros. uniformRandVarU = zeros(365,24)
2. Set randVarX to be equal to grouped data
3. Begin a *for* loop with size $s = 24$. (If the analysis is not daily UC or if the UC is not done hourly, the size could be different)
4. Compute the marginal empirical cdf using the function ksdensity in Matlab. uniformRandVarU(:,s) = ksdensity(randVarX(:,s), randVarX(:,s),'function','cdf','Bandwidth',2);
5. End of *for* loop
6. Compute correlation between the marginals generated in step 4. *rho* = copulafit('Gaussian',uniformRandVarU)
7. Generate random samples of a standard multivariate normal distribution using *rho* and compute the cdf in one function. copulGRandU = copularnd('Gaussian', *rho*,Nsamples), where Nsamples is the number of samples that is to be generated
8. Begin a *for* loop with size $s = 24$
9. Compute the inverse cdf using the function ksdensity in Matlab. Sampled(:,s) = ksdensity(randVarX(:,s),copulGRandU(:, s),'function','icdf','Bandwidth',2)
10. End of *for* loop

4.1. Assessing the importance of scenarios for scenario selection

Our goal is to select a number of representative scenarios that characterize the system uncertainty as precisely as possible, given a fixed (maximum) number of scenarios that can be used. To accomplish this, a mathematical tool, the Kantorovich distance, that assesses the importance of a given scenario is used. The Kantorovich distance is used to rank the scenarios. The ranking score is then used to map the scenarios into a 3-dimensional space. First a matrix of distances is created as shown in Eq. (29).

$$K_m = \begin{bmatrix} (|\widetilde{\xi}_1^p(1) - \widetilde{\xi}_1^p(1)| + \ldots + |\widetilde{\xi}_T^p(1) - \widetilde{\xi}_T^p(1)|) & \cdots & (|\widetilde{\xi}_1^p(1) - \widetilde{\xi}_1^p(K)| + \ldots + |\widetilde{\xi}_T^p(1) - \widetilde{\xi}_T^p(K)|) \\ \vdots & \ddots & \vdots \\ (|\widetilde{\xi}_1^p(K) - \widetilde{\xi}_1^p(1)| + \ldots + |\widetilde{\xi}_T^p(K) - \widetilde{\xi}_T^p(1)|) & \cdots & (|\widetilde{\xi}_1^p(K) - \widetilde{\xi}_1^p(K)| + \ldots + |\widetilde{\xi}_T^p(K) - \widetilde{\xi}_T^p(K)|) \end{bmatrix} \tag{29}$$

where $K = |\Omega|$ i.e., K is the number of scenarios in the uncertainty space including all scenarios.

The Kantorovich distance is then given as

$$K_d = K_m \pi_\omega \tag{30}$$

where π_ω is a column vector of scenario probability. Note that the scenarios have equal probability. Thus,

$$\pi_\omega = \begin{bmatrix} \frac{1}{K} \\ \vdots \\ \frac{1}{K} \end{bmatrix} \tag{31}$$

The procedure for ranking the scenarios is explained as follows:

1. Calculate a matrix of distances for all the scenarios using Eq. (29) and calculate the Kantorovich distance using Eq. (30)
2. Find the scenario with the minimum Kantorovich distance and assign it a rank *h*.
3. Update the matrix of distances in Eq. (29) by comparing the distances of the *h*-th scenario (column vector) in step 2 with the distances of all the scenarios (column vector) and choose the minimum distance for each entry.
4. Additionally, update the matrix of distances by replacing the *h*-th row with the distances of the *h*-th scenario in step 2.
5. Go to step 2 if all the scenarios have not been selected. Go to step 6 if all the scenarios have been selected.
6. Calculate the rank score for all the scenarios.

The rank score for a scenario ranked *h*-th out of K scenarios is given by

$$t(\xi^p(\omega)) = \frac{h-1}{K-1} \tag{32}$$

where $t(\xi^p(\omega)) \rightarrow 1$ is for scenarios that can be regarded as more repre-

sentative while $t(\xi^p(\omega))\rightarrow 0$ is for scenarios that are regarded as less representative. The rank score is used to map the random variable to a 3-dimensional space. Each profile of load, wind speed and solar irradiation are joined together to form scenarios. This mapping not only preserves the information that has been observed for the distribution of each random variable, but also captures different profile combination that could happen despite not having been observed before.

The Matlab code for the ranking of the scenarios using Kantorovich distance is made available in [45].

4.2. Methodology for the joining of the load, wind and solar profiles to form scenarios

After the load, wind and solar profiles have been given a rank score using the Kantorovich distance method in section 4.1 they are then joined together using a novel method developed in this paper. The rank score is divided into three segments: low rank ("low") which is from 0 to 0.333, medium rank ("med") which is from 0.334 to 0.666 and high rank ("high") which is from 0.667 to 1. All the rank variables are, thus: load high, load medium and load low, wind high, wind medium and wind low, solar high, solar medium and solar low. Scenarios are then formed using all the permutations of the rank (27 permutations).

For each permutation a random number is generated in the rank range which is used to select the profile that has a value closest to this generated random number. For example, for load high, wind low, solar medium, a random number is generated between 0.667 and 1 for load, 0 to 0.333 for wind and 0.334 to 0.666 for solar. Once a profile has been selected, it is removed from the matrix to ensure that no profile is selected twice. This way the scenarios are guaranteed to have all the likely profiles that can be encountered. In this work 1000 scenarios are generated. Using this method, the 27 permutations run 37 times to form 999 scenarios. The last profile of load, wind speed and solar irradiation are joined together to form the last scenario.

4.3. Scenario clustering

After the profiles have been assigned a rank score and joined together to form scenarios, the multivariate data points $(\widetilde{\xi}^l, \widetilde{\xi}^w, \widetilde{\xi}^{pv})$ from (F^l, F^w, F^{pv}) representing a sampled scenario are mapped into a 3-dimensional space. They are then clustered together to form a reduced scenario set, whose elements are the centroids of the clusters. There are many scenarios clustering method, but the k-means method has been used in this work. The following expresses the k-means method:

$$\min_{r,\mu} \sum_{m=1}^{K} \sum_{n=1}^{K_{rd}} r_{mn} \|\boldsymbol{x_m} - \boldsymbol{\mu_n}\|_2^2 \tag{33}$$

s.t., $\boldsymbol{x_m} = \left(t_m(\widetilde{\xi}^l(\omega)), t_m(\widetilde{\xi}^w(\omega)), t_m(\widetilde{\xi}^{pv}(\omega))\right)$ where $r_{mn} \in \{0,1\}$, K_{rd} is the number of elements of the reduced scenario set. Solving Eq. (33) returns the clusters and the associated centroids $\boldsymbol{\mu_n}$.

5. Determination of optimal ES size

The algorithm for determining the optimal ES size is illustrated in the flow chart in Fig. 2. The algorithm begins with the setting of the minimum and maximum BESS capacity. The minimum BESS capacity is set to 0 MWh and the maximum BESS capacity is set to a reasonably large number to select a reasonable search space. Then the selected scenarios are integrated in the SUC model and the parameters and initial variables are set. The BESS capacity is then set to the minimum BESS capacity. The SUC is then solved to find the *TUCC* (minimize TUCC in Eq. (1)). The algorithm then checks if the BESS capacity is less than the maximum BESS capacity. If the BESS capacity is less than the maximum BESS capacity, the algorithm increases the BESS capacity by a defined step increase, and solves the SUC again. The algorithm then checks again if the BESS capacity is less than the maximum BESS capacity. The process continues until the BESS capacity is no longer less than the maximum BESS capacity at which point the algorithm ends. The *TUCC* is then plotted against the BESS capacity and the BESS capacity with the least *TUCC* is the optimal BESS capacity.

6. Case study

We consider sizing BESS for spinning reserve and efficiency increase on a real OOGP in the North Sea. The OOGP has four GTGs. The OOGP is an isolated power system and high energy security is often guaranteed by using GTGs to provide sufficient spinning reserve. Using BESS can help turn off one GTG leading to cost and carbon emissions reduction. The SUC model presented in section 3 is used to size the BESS. In this case study, it is assumed that the OOGP is integrated with WTs and solar PV panels. In this case study 2 WTs rated at 8.6 MW each (17.2 MW in total) and an offshore solar farm rated at 8.6 MW is assumed to be integrated with the OOGP. The data for the GTGs is provided in Table A1 in Appendix A. The number of scenarios in the reduced scenario subset is chosen as 50.

The first step is to generate the scenarios. 1000 profiles are generated for load, wind speed and solar irradiation using the copula-based method described in section 4. Figs. 3–5 show the generated profiles for load, wind speed and solar irradiation, which are the profiles out of which 50 profiles are selected using scenario reduction. Then the rank for each profile in Figs. 3–5 is calculated using the Kantorovich distance introduced in section 4. Note that the rank is calculated using only profiles belonging to a particular uncertainty i.e. the rank for load is different from that of the wind speed or solar irradiation. After the rank has been calculated for all the profiles, the method described in section 4.2 is then used to join the profiles (using the rank score) to form scenarios. Then the scenarios are plotted in a 3- dimensional space using the rank for each profile in a scenario. Note that a scenario contains one profile of load, one profile of wind speed and one profile of solar irradiation. Fig. 6 shows the plot of the 3-dimensional rank space containing 1000 scenarios and the 50 centroids. The scenario closest to each centroid in Fig. 6 is selected for the 50 centroids. Thus, we get 50 scenarios with each scenario consisting of a profile of load, wind speed and solar irradiation.

The 50 profiles that were selected for load, wind speed and solar irradiation after scenario reduction are shown in Figs. 7–9. Once the profiles have been selected, they can then be used in the SUC problem to determine the optimal ES size.

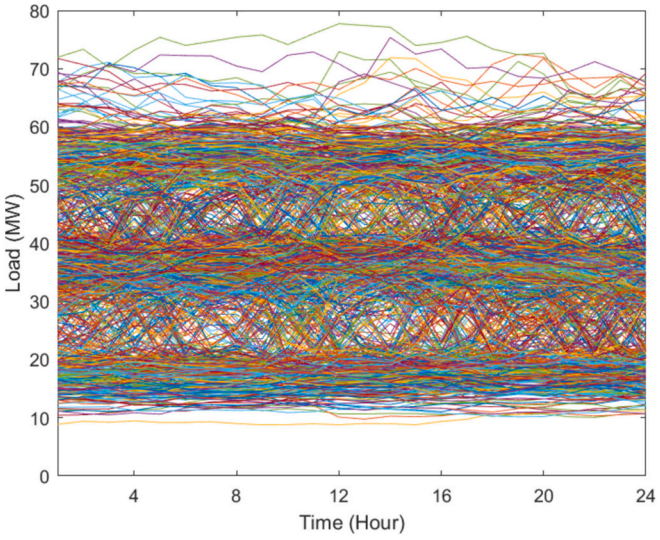

Fig. 3. 1000 generated load profiles. Each colour represents one profile.

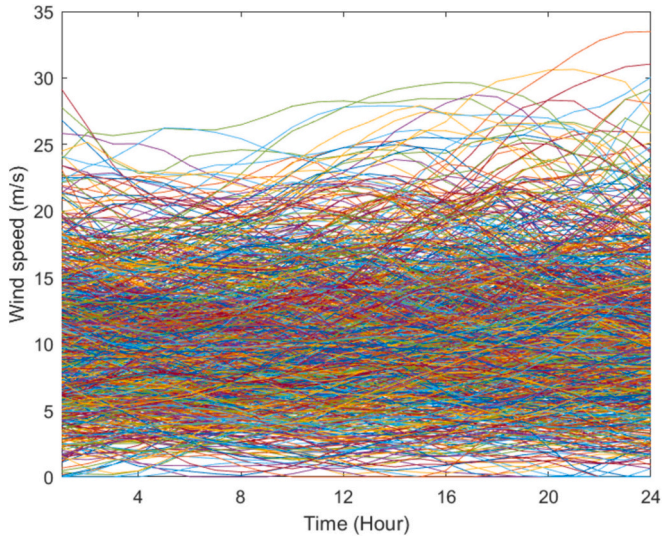

Fig. 4. 1000 generated wind speed profiles. Each colour represents one profile.

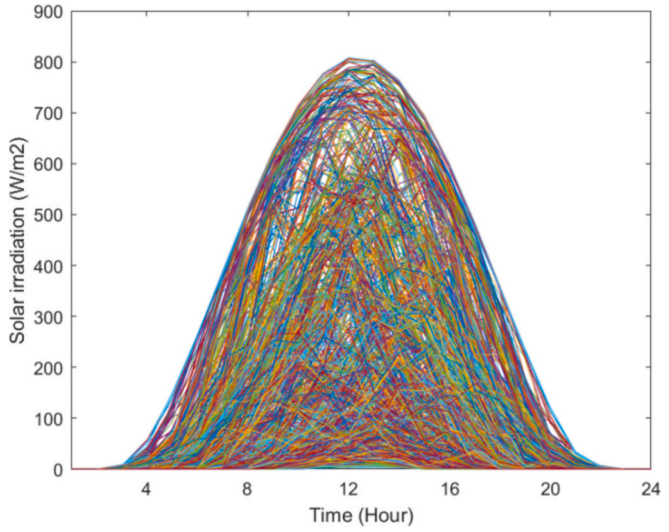

Fig. 5. 1000 generated solar irradiation profiles. Each colour represents one profile.

To demonstrate that the scenario reduction technique presented in section 4 preserves the statistical properties of the larger dataset, the hourly average and standard deviation of the load demand, wind speed and solar irradiation are shown Tables 2–7. The hourly average for load demand, wind speed and solar irradiation is calculated using Eqs. (34) and (35). Note that in Eqs. (34) and (35) the scenario probability is used to calculate the hourly average.

$$AH_t^p = \sum_{g=1}^{G} \widetilde{\xi}_t^p(g) \bullet \pi_g \tag{34}$$

$$Ah_t^p = \sum_{v=1}^{V} \widetilde{\xi}_t^p(v) \bullet \pi_v \tag{35}$$

where AH_t^p is the average hourly load demand, wind speed or solar irradiation when the number of scenarios is 1000, G is the number of scenarios which is 1000, Ah_t^p is the average hourly load demand, wind speed or solar irradiation when the number of scenarios is 50, V is the number of scenarios which is 50, π_g is the scenario probability when the number of scenarios is 1000 i.e. $\omega = g$ when the number of scenarios is 1000 and π_v is the scenario probability for a scenario when the number of scenarios is 50, i.e. $\omega = v$ when the number of scenarios is 50. Thus, $\widetilde{\xi}_t^p(\omega) = \widetilde{\xi}_t^p(g)$ and $\pi_\omega = \pi_g$ for 1000 scenarios and $\widetilde{\xi}_t^p(\omega) = \widetilde{\xi}_t^p(v)$ and $\pi_\omega = \pi_v$ for 50 scenarios.

The hourly standard deviation for load demand, wind speed or solar irradiation is calculated using Eqs. (36) and (37).

$$SH_t^p = \sqrt{\sum_{g=1}^{G} \left(\widetilde{\xi}_t^p(g) - AH_t^p\right)^2 \bullet \pi_g} \tag{36}$$

$$Sh_t^p = \sqrt{\sum_{v=1}^{V} \left(\widetilde{\xi}_t^p(v) - Ah_t^p\right)^2 \bullet \pi_v} \tag{37}$$

where SH_t^p is the hourly standard deviation for load demand, wind speed or solar irradiation when the number of scenarios is 1000 and Sh_t^p is the hourly standard deviation for load demand, wind speed or solar irradiation when the number of scenarios is 50.

Note that for the 1000 generated scenarios, the scenario probability, π_g, is the same for all the scenarios but the scenario probability, π_v, is different for the 50 selected scenarios.

The average hourly load demand, wind speed and solar irradiation for the 1000 generated scenarios and 50 selected scenarios are shown in Tables 2–4. It can be seen that the difference in value between the average hourly load demand, wind speed and solar irradiation of the 1000 generated scenarios and the 50 selected scenarios is not significant. The average hourly standard deviation of the load demand, wind speed and solar irradiation for the 1000 generated scenarios and 50 selected scenarios are shown in Tables 5–7. It can be seen that the difference in value between the hourly standard deviation for the load demand, wind speed and solar irradiation of the 1000 generated scenarios and the 50 selected scenarios is not significant, either. The closeness of the statistical properties (hourly average and hourly standard deviation) of the 1000 generated scenarios and the 50 selected scenarios shows that the scenario reduction technique does preserve the statistical properties of the large dataset (generated scenarios) in the few selected scenarios.

6.1. Test cases

Five test cases are considered in the ES sizing. The test cases are shown in Table 8. The base test case is case S1. In case S4 where battery degradation is not considered a life span of 12.5 years is assumed for the LFP battery.

7. Results and discussions

The main aim in this section is to find the optimal BESS capacity for the test cases with BESS and to subsequently find out which test case yields the lowest TUCC. Also, we perform sensitivity analysis to find out how the TUCC varies with BESS capacity cost in the test cases with BESS and how the optimal BESS capacity varies with increased renewable penetration. The problem is solved using MILP in gurobi and Matlab

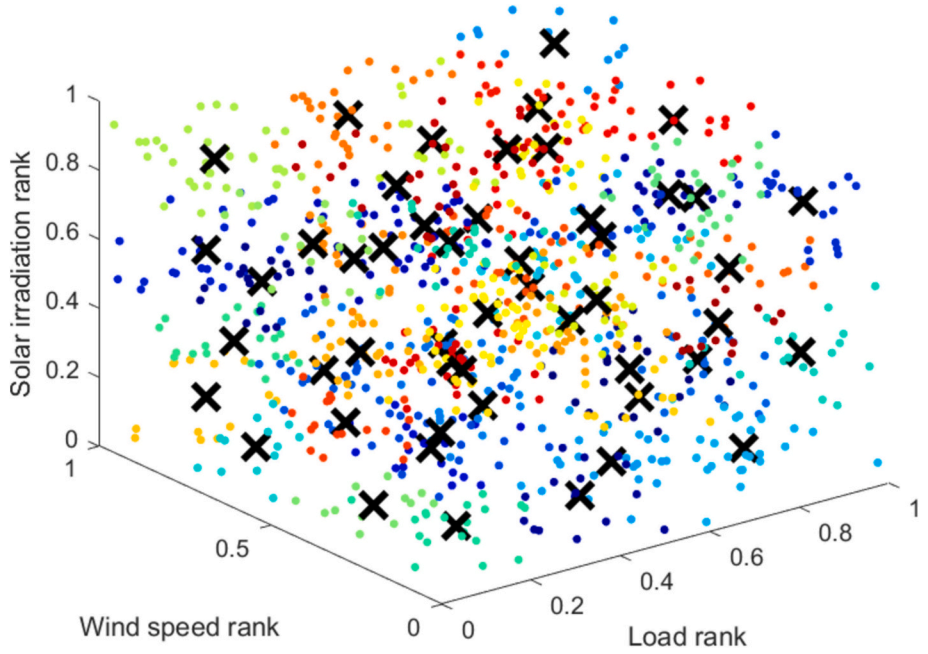

Fig. 6. Figure showing the generated 1000 scenarios in the 3-dimensional rank space. Randomly sampled profiles (load, wind speed and solar irradiation) are represented as points in the 3-dimensional rank space and grouped into 50 groups, the centroids of which make up the reduced scenario subset Ω_s. Different colours correspond to different clusters

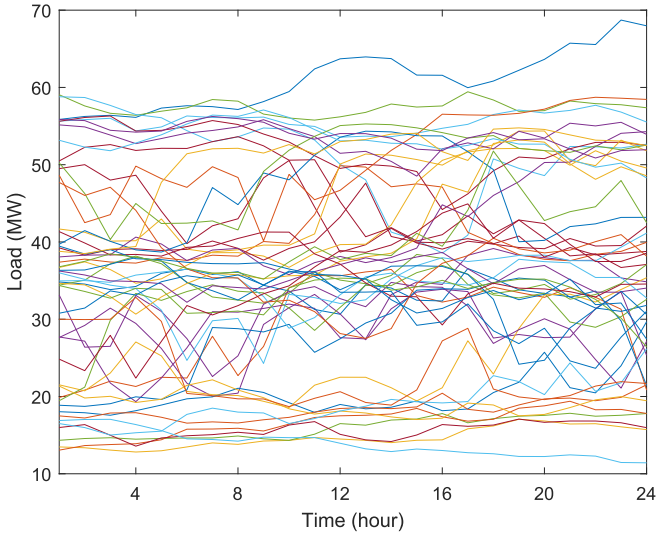

Fig. 7. 50 profiles of load selected after scenario reduction.

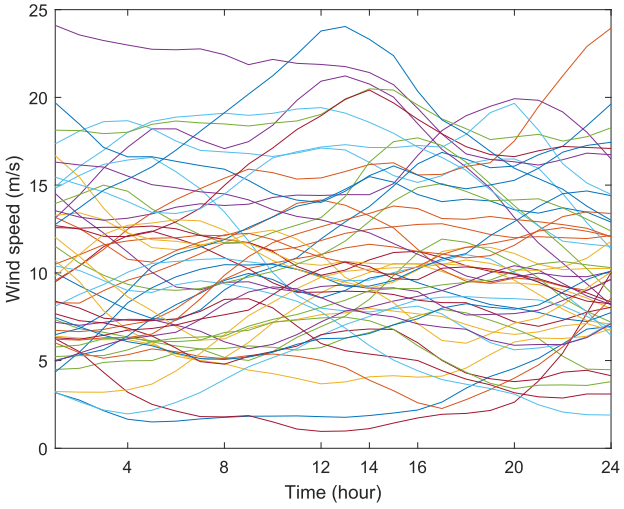

Fig. 8. 50 profiles of wind speed selected after scenario reduction.

interface on a PC with 2.6 GHz Intel Core i5-1145G7 and 16 GB RAM.

7.1. Determination of optimal BESS size

The TUCC is calculated for BESS sizes in the range 0–50 MWh. The BESS size is increased by 2.5 MWh from 0 MWh to 50 MWh. The optimal BESS capacity is only determined for cases S3, S4 and S5 as these are the cases that include BESS. The TUCC is plotted against varying BESS capacities in cases S3, S4 and S5 in Fig. 10.

Table 9 shows the TUCC, carbon emissions, efficiency (average efficiency of the GTGs over a period of one day) and expected energy produced for the case S1, S2 and for the optimal BESS capacity in case S3, S4 and S5. Note that the carbon footprint of the BESS is included in the total carbon emissions (along with the GTG carbon emissions). The carbon footprint includes all the carbon emissions associated with production of the battery, and the emissions associated with recycling of the battery. A carbon footprint of 100 $kgCO_2$/kWh is used [46]. The carbon footprint per day is calculated using the life span of the BESS. In the cases that included battery degradation (cases S3 and S5) the life span is derived from the UC model. It can be seen in Fig. 10 that the optimal BESS capacity in case S3, S4 and S5 are 42.5 MWh, 27.5 MWh and 40 MWh respectively. However, deploying a BESS of large capacity in an offshore platform can be difficult and expensive due to the limited

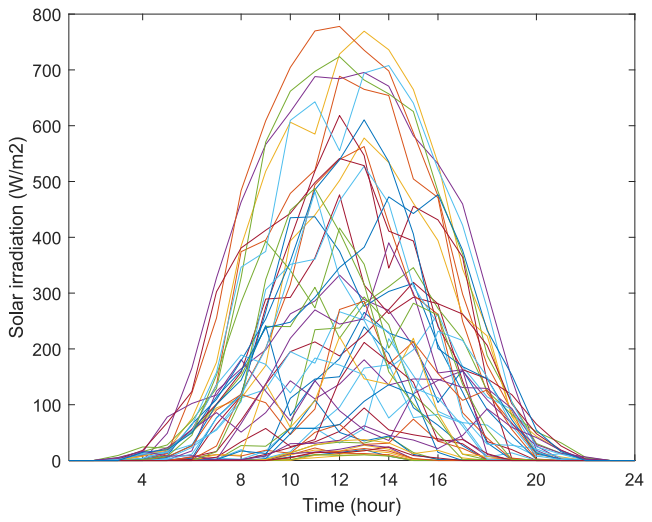

Fig. 9. 50 profiles of solar irradiation selected after scenario reduction.

weight and space that the offshore platform can accommodate. In this work, we have not considered how the BESS will be deployed but we can assume that a high BESS capacity may not be the best choice as a new floating platform may be needed if the BESS capacity is large thus making the BESS deployment expensive. Thus, smaller BESS capacities that have cost reduction closer to that of the optimal capacity are considered the most practical BESS capacity which explains why the optimal BESS capacities are not identified in Fig. 10. Thus, the most practical (near-optimal) BESS capacity in S3, S4 and S5 are 35 MWh, 27.5 MWh and 27.5 MWh respectively.

The UC schedules for the near-optimal BESS capacity in cases S1, S3 and S5 are shown in Tables 10–12. The near-optimal BESS capacity in S4 has the same UC schedule as the one in S5 so it is not shown. Also, the UC schedule in S2 is the same as the one in S1 so it is not shown. In Table 10–12, 1 signifies "on" status and 0 signifies "off" status. It can be seen in Table 11 that 2 GTs are on in hours 2, 8, 9, 13, 14, 15, 19 and 20 as opposed to the schedule in S1 which has 3 GTGs on for all hours. It can be seen in Table 12 that 2 GTGs are on in hours 4, 5, 11, 12, 13, 16, 17 and 18 as opposed to S1, which has 3 GTGs on for all hours. The turning off of one GTG in the results of S3, S4 and S5 for the near-optimal BESS capacity allows significant reduction of TUCC and carbon emissions.

It can be seen from Table 9 that the efficiency increased when BESS and flexible load are used, thus, the operation of the GTGs at partial loads is reduced. Even though the increase in efficiency in cases S3, S4 and S5 is not large, the cost and carbon emissions reduction are significant as the expected energy produced is lower in cases S3, S4 and S5 compared to case S1. The reduction in expected energy produced when BESS and flexible load are used is due to the scenarios where minimum generation is higher than the net load and energy is wasted in a dump

Table 2
Average hourly load demand for the 1000 generated scenarios and 50 selected scenarios.

Hour	1	2	3	4	5	6	7	8	9	10	11	12
AL-1000 (MW)	37.24	37.28	37.29	37.32	37.38	37.28	37.35	37.33	37.2	37.15	37.25	37.17
AL-50 (MW)	36.06	35.7	35.69	35.89	35.85	35.42	36.1	35.98	36.31	36.76	36.76	36.81
Hour	13	14	15	16	17	18	19	20	21	22	23	24
AL-1000 (MW)	37.19	37.29	37.33	37.3	37.3	37.34	37.34	37.35	37.13	37.11	37.24	37.05
AL-50 (MW)	36.99	37.12	37.39	37.79	38.18	38.32	38.14	38.19	38.02	37.74	38.18	37.99

AL-1000 means average hourly load demand for 1000 generated scenarios, AL-50 means average hourly load demand for the 50 selected scenarios.

Table 3
Average hourly wind speed for the 1000 generated scenarios and 50 selected scenarios.

Hour	1	2	3	4	5	6	7	8	9	10	11	12
AW-1000 (m/s)	10.32	10.24	10.2	10.16	10.11	10.1	10.12	10.16	10.22	10.32	10.42	10.51
AW-50 (m/s)	10.21	10.18	10.18	10.2	10.25	10.31	10.4	10.58	10.73	10.81	10.86	10.97
Hour	13	14	15	16	17	18	19	20	21	22	23	24
AW-1000 (m/s)	10.59	10.63	10.66	10.67	10.68	10.72	10.72	10.72	10.72	10.72	10.69	10.67
AW-50 (m/s)	11.11	11.2	11.22	11.05	10.88	10.73	10.6	10.54	10.53	10.49	10.49	10.49

AW-1000 means average hourly solar irradiation for 1000 generated scenarios, AW-50 means average hourly solar irradiation for the 50 selected scenarios.

Table 4
Average hourly solar irradiation for the 1000 generated scenarios and 50 selected scenarios.

Hour	1	2	3	4	5	6	7	8	9	10	11	12
AS-1000 (W/m^2)	0	0	0.4	3.8	11.5	35	72.4	126.1	179.3	221.1	254.5	273
AS-50 (W/m^2)	0	0	0.53	3.4	9.1	27.6	65.1	114.7	166.3	209	247.5	266.8
Hour	13	14	15	16	17	18	19	20	21	22	23	24
AS-1000 (W/m^2)	275.1	250.3	217	171.9	114	68.3	33.2	10.6	2.9	0.3	0	0
AS-50 (W/m^2)	270.8	248.4	220.5	174.2	123	73.5	35.2	10.1	3.7	0.4	0	0

AS-1000 means average hourly solar irradiation for 1000 generated scenarios, AS-50 means average hourly solar irradiation for the 50 selected scenarios.

Table 5
Hourly standard deviation for load demand for the 1000 generated scenarios and 50 selected scenarios.

Hour	1	2	3	4	5	6	7	8	9	10	11	12
SL-1000 (MW)	14.62	14.61	14.47	14.42	14.49	14.56	14.65	14.69	14.54	14.54	14.56	14.63
SL-50 (MW)	13.93	13.75	13.37	13.27	13.19	13.43	13.55	13.49	13.46	13.48	13.27	13.34
Hour	13	14	15	16	17	18	19	20	21	22	23	24
SL-1000 (MW)	14.59	14.67	14.48	14.35	14.37	14.48	14.44	14.49	14.54	14.72	14.65	14.71
SL-50 (MW)	13.55	13.28	13.01	12.9	12.78	13.58	13.38	13.13	13.3	13.51	13.64	13.34

SL-1000 means hourly standard deviation for load demand for 1000 generated scenarios, SL-50 means hourly standard deviation for load demand for the 50 selected scenarios.

Table 6
Hourly standard deviation for wind speed for the 1000 generated scenarios and 50 selected scenarios.

Hour	1	2	3	4	5	6	7	8	9	10	11	12
SW-1000 (m/s)	4.66	4.56	4.47	4.44	4.46	4.5	4.55	4.61	4.68	4.8	4.88	4.95
SW-50 (m/s)	4.65	4.62	4.64	4.69	4.76	4.75	4.69	4.62	4.56	4.63	4.78	4.95
Hour	13	14	15	16	17	18	19	20	21	22	23	24
SW-1000 (m/s)	4.97	4.98	5.02	5.04	5.1	5.15	5.15	5.11	5.11	5.12	5.13	5.06
SW-50 (m/s)	5.06	5.06	4.96	4.77	4.68	4.64	4.58	4.6	4.61	4.59	4.6	4.61

SW-1000 means hourly standard deviation for wind speed for 1000 generated scenarios, SW-50 means hourly standard deviation for wind speed for the 50 selected scenarios.

Table 7
Hourly standard deviation for solar irradiation for the 1000 generated scenarios and 50 selected scenarios.

Hour	1	2	3	4	5	6	7	8	9	10	11	12
SS-1000 (W/m^2)	0	0	1.3	8.2	23	55.8	98.4	146.7	186	210.2	229.2	239.5
SS-50 (W/m^2)	0	0	1.5	5.9	16.6	40.4	83.3	137.3	179.7	216.8	231.3	242.6
Hour	13	14	15	16	17	18	19	20	21	22	23	24
SS-1000 (W/m^2)	235.1	221.1	202.8	174.4	132.5	91.6	50.5	19.9	6.3	1	0	0
SS-50 (W/m^2)	240.8	225	203.5	175.1	135.1	88.8	45.5	16.9	7.1	1.3	0	0

SS-1000 means hourly standard deviation for solar irradiation for 1000 generated scenarios, SS-50 means hourly standard deviation for solar irradiation for the 50 selected scenarios.

Table 8
The test cases considered in this paper.

Case	**Description**
Case S1	SUC without BESS and flexible load
Case S2	SUC with flexible load and no BESS
Case S3	SUC with BESS (with detailed battery degradation modelling) and no flexible load
Case S4	SUC with BESS (with imprecise cost estimation) and flexible load
Case S5	SUC with BESS (with detailed battery degradation modelling) and flexible load

load. However, with BESS and flexible load, the energy wasted in dump load is reduced when net load is lower than minimum generation as energy can be stored in the BESS and flexible load power can be increased and when net load is more than minimum generation the energy can be discharged from the BESS and flexible load power can be reduced. Net load refers to load demand minus renewable generation. Minimum generation refers to minimum power that must be produced by the GTGs running.

The results show that the methodology proposed in this work allows us to size a BESS for an isolated power system with multiple

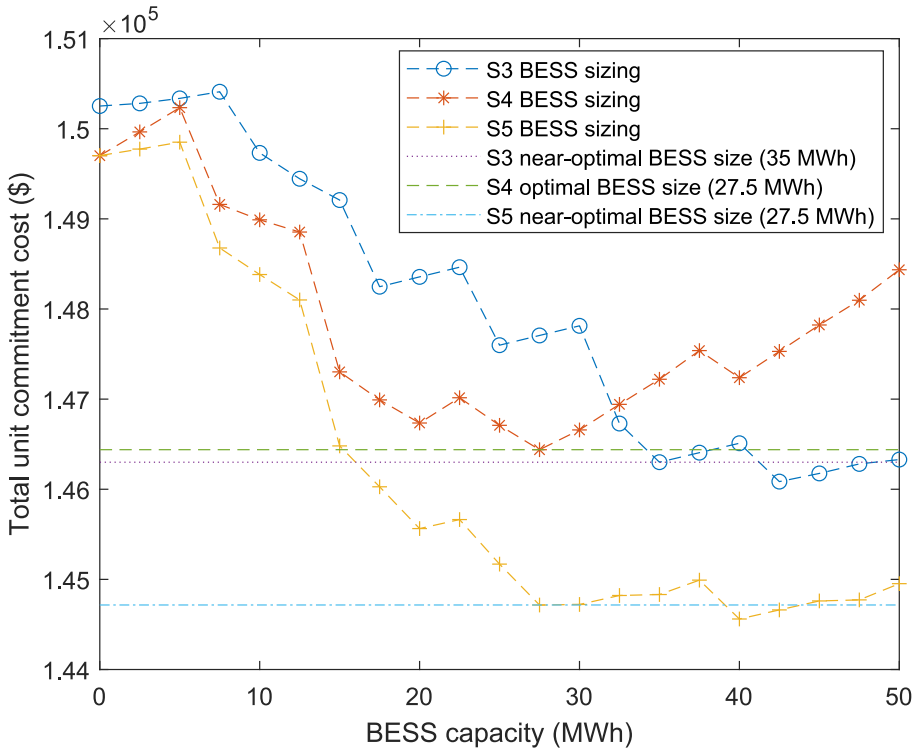

Fig. 10. Plot of the TUCC for BESS sizes from 0 MWh to 50 MWh.

Table 9
TUCC, CO_2 emissions, cost reduction, CO_2 emissions reduction, efficiency, expected energy produced and spinning reserve margin in cases S1, S2 and at near-optimal BESS capacity in cases S3, S4 and S5.

Case	S1 (base case)	S2	S3 (Near-optimal BESS capacity)	S4 (Optimal BESS capacity)	S5 (Near-optimal BESS capacity)
TUCC	$150,252	$149,702	$146,300	$146,439	$144,716
CO_2 emissions	511,620 kg	509,748 kg	491,748 kg	488,977 kg	488,595 kg
Cost reduction with respect to base case (S1)	0 %	0.37 %	2.63 %	2.54 %	3.68 %
CO_2 emissions reduction with respect to base case (S1)	0 %	0.37 %	3.88 %	4.43 %	4.5 %
Efficiency	27.94 %	27.88 %	28.93 %	28.89 %	28.89 %
Expected energy produced by the GTGs	696.18 MWh	692.19 MWh	681.19 MWh	679.01 MWh	678.92 MWh
Spinning reserve margin	52.13 %	57.36 %	51.99 %	53.65 %	55.59 %

uncertainties such that the sized BESS is statistically stable i.e. the BESS capacity can introduce flexibility that allows the system to cope with wide range of scenarios and uncertainties leading to no loss of load, less wasted energy and increased average operational efficiency leading to significant cost and carbon emissions reduction. Thus, this methodology can be applied to any case study of an isolated power system.

It can also be seen from Table 9 that the modelling of the battery degradation allows increased reduction in TUCC. This is because the accurate modelling of the battery degradation results in an increased lifespan of the battery which leads to reduced battery cost. The reduction in TUCC in cases S4 and S5 are 2.54 % and 3.68 % respectively but the battery cost reduction is more than these numbers suggest. In fact, there is about 57 % reduction in the cost of the battery when the battery degradation is modelled in S5 compared to the case with imprecise cost estimation in S4 (without detailed degradation modelling).

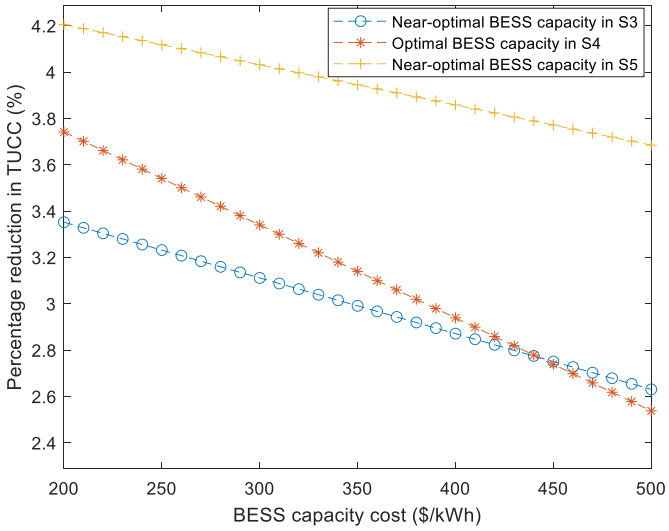

Fig. 11. Percentage reduction in TUCC in near-optimal BESS capacity in cases S3, S4 and S5 compared to case S1, against BESS capacity cost.

It can also be seen from Table 9 that the inclusion of BESS and flexible load in S4 and S5 allows maintaining the spinning reserve margin above the level in the base case (S1) while also improving the efficiency of the GTGs. The spinning reserve margin in S3 was also maintained at almost the same value as the margin in S1 while also improving the efficiency of the GTGs.

7.2. Sensitivity analysis

7.2.1. Sensitivity to BESS capacity cost

Here the sensitivity of the TUCC to BESS capacity cost is assessed. Since cost of batteries are expected to further reduce in the future, it is good to examine how much reduction in BESS capacity cost will impact the reduction in TUCC. For the purpose of this analysis the TUCC is examined at the near-optimal BESS capacities in cases S3, S4 and S5 for a

Table 10
Unit commitment schedule for case S1.

Hour	1	2	3	4	5	6	7	8	9	10	11	12	13	14	15	16	17	18	19	20	21	22	23	24
GTG1	1	1	1	1	1	1	1	1	1	1	1	1	1	1	1	1	1	1	1	1	1	1	1	1
GTG2	1	1	1	1	1	1	1	1	1	1	1	1	1	1	1	1	1	1	1	1	1	1	1	1
GTG3	1	1	1	1	1	1	1	1	1	1	1	1	1	1	1	1	1	1	1	1	1	1	1	1
GTG4	0	0	0	0	0	0	0	0	0	0	0	0	0	0	0	0	0	0	0	0	0	0	0	0

Table 11
Unit commitment schedule for near-optimal BESS capacity (35 MWh) in case S3.

Hour	1	2	3	4	5	6	7	8	9	10	11	12	13	14	15	16	17	18	19	20	21	22	23	24
GTG1	1	1	1	1	1	1	1	1	1	1	1	1	1	1	1	1	1	1	1	1	1	1	1	1
GTG2	1	1	1	1	1	1	1	1	1	1	1	1	1	1	1	1	1	1	1	1	1	1	1	1
GTG3	1	0	0	0	0	0	0	0	0	1	1	1	0	0	0	1	1	1	0	0	0	0	0	0
GTG4	0	0	1	1	1	1	1	0	0	0	0	0	0	0	0	0	0	0	0	0	1	1	1	1

Table 12
Unit commitment schedule for near-optimal BESS capacity (27.5 MWh) in case S5.

Hour	1	2	3	4	5	6	7	8	9	10	11	12	13	14	15	16	17	18	19	20	21	22	23	24
GTG1	1	1	1	1	1	1	1	1	1	1	1	1	1	1	1	1	1	1	1	1	1	1	1	1
GTG2	1	1	1	1	1	1	1	1	1	1	1	1	1	1	1	0	0	0	1	1	1	1	1	1
GTG3	1	1	1	0	0	0	0	0	0	0	0	0	0	1	1	1	1	1	1	1	1	1	1	1
GTG4	0	0	0	0	0	1	1	1	1	1	0	0	0	0	0	0	0	0	0	0	0	0	0	0

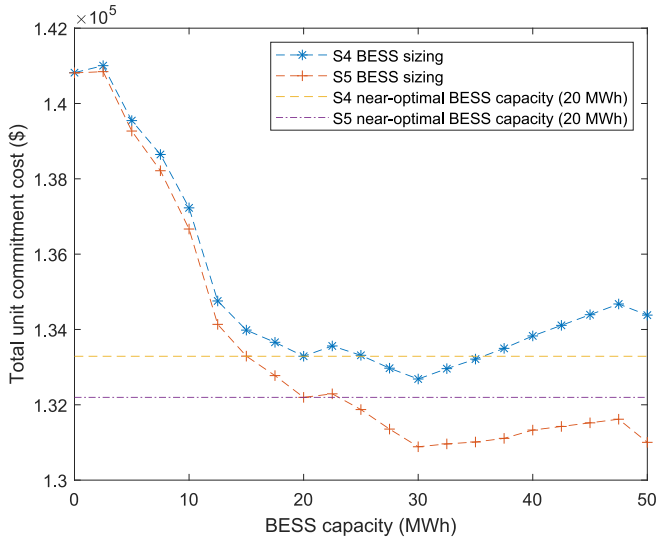

Fig. 12. Plot of the TUCC for BESS sizes from 0 MWh to 50 MWh.

Table 13
TUCC, CO_2 emissions, cost reduction, CO_2 emissions reduction, efficiency, expected energy produced and spinning reserve margin in cases S1, S2 and at near-optimal BESS capacity in cases S4 and S5.

Case	S1 (base case)	S2	S4 (Near-optimal BESS capacity)	S5 (Near-optimal BESS capacity)
TUCC	$141,753	$140,812	$133,289	$132,198
CO_2 emissions	482,682 kg	479,477 kg	446,836 kg	446,599 kg
Cost reduction with respect to base case (S1)	0 %	0.66 %	5.97 %	6.74 %
CO_2 emissions reduction with respect to base case (S1)	0 %	0.66 %	7.43 %	7.48 %
Efficiency	26.94 %	26.83 %	28.06 %	28.06 %
Expected energy produced by the GTGs	633.42 MWh	626.51 MWh	596.69 MWh	596.65 MWh
Spinning reserve margin	56.45 %	61.87 %	56.08 %	57.56 %

change in BESS capacity cost from $500/kWh to $200/kWh.

Fig. 11 shows the plot of the percentage reduction in TUCC for the near-optimal BESS capacity in cases S3, S4 and S5 compared to case S1 against the BESS capacity cost. It can be seen that for the three cases there is an increase in percentage reduction in TUCC but the optimal BESS capacity in case S4 shows the biggest impact of falling battery capacity cost on the TUCC. The percentage reduction in TUCC in the near-optimal BESS capacity in cases S3, S4 and S5 increased from 2.63 % to 3.35 %, 2.54 % to 3.74 % and 3.68 % to 4.2 % respectively as battery capacity cost reduces from $500/kWh to $200/kWh. The reason for limited impact of the battery capacity cost on the TUCC is because the BESS cost/BESS degradation cost is a small fraction of the TUCC.

7.2.2. Sensitivity to renewable penetration

Here, we consider the impact of the renewable penetration on the optimal BESS size. We run the BESS sizing algorithm for an OOGP with three 8.6 MW WTs (25.8 MW in total) and 12.9 MW solar farm to see how a higher renewable penetration affects the optimal BESS size. In this section, only cases S1, S2, S4 and S5 are investigated. Fig. 12 shows the plot of the BESS size against the TUCC. Table 13 shows the TUCC, CO_2 emissions, cost reduction, CO_2 emissions reduction, efficiency, expected energy produced by the GTGs and the spinning reserve margin.

From Fig. 12 we can see that the optimal BESS capacity in cases S4 and S5 is 30 MWh, however, we have chosen 20 MWh because it is a near-optimal solution, and we consider it to be the most practical choice.

The result of this sizing shows that increasing the renewable penetration changes the optimal BESS size. However, the most significant outcome is not the change in the optimal BESS size at higher renewable penetration but the higher cost reduction and carbon emissions reduction which can be seen in Table 13. This suggests that BESS integration with OOGP has higher benefits at higher renewable penetration and as such should be prioritized. As with the base test case, the expected energy produced is lower in the cases with BESS than the cases without BESS which helps increase the reduction in cost and carbon emissions. We can also see that the spinning reserve margin was maintained when BESS is used compared to the case without BESS which guarantees security of power supply. The UC schedule for case S1 and S2 in the test case in this section is the same as the one in Table 10. The UC schedule for case S5 is shown in Table 14. Case S4 has the same UC schedule as case S5.

7.3. Final remarks

In this work, the recommended solution for the case study (an OOGP in the North Sea) is the near-optimal BESS capacity in case S5 as this has the lowest TUCC while it has more CO_2 emissions reduction than the optimal result in case S4. Thus, the best solution is a BESS capacity of 27.5 MWh and smart load management of a flexible load of 6 MW.

However, if the renewable penetration increases a 20 MWh BESS and smart load management of a flexible load of 6 MW can be a good solution. The optimal BESS capacity of 30 MWh is not chosen because the incremental benefits over the 20 MWh solution is not significant keeping in mind that deployment of large BESS capacity in OOGP is complicated due to limited weight and space allowed in OOGPs.

From the results of this work three main points are highlighted:

- An accurate value for the optimal BESS capacity can be found for an isolated power system using the methodology proposed in this work.
- In general, this result confirms that for any case study the optimal BESS capacity can be reduced if load-shifting DR can be applied to some loads as was done in [39].
- The result of this work also highlights the significance of modelling battery degradation in SUC formulations as cost reduction increased from 2.54 % to 3.68 % when battery degradation is modelled.

8. Conclusion

This work proposed a method for sizing battery energy storage system for spinning reserve and a more efficient operation of the thermal power plants (diesel generators, gas turbine generators) in isolated

Table 14
Unit commitment schedule for near-optimal BESS capacity (20 MWh) in case S5.

Hour	1	2	3	4	5	6	7	8	9	10	11	12	13	14	15	16	17	18	19	20	21	22	23	24
GTG1	1	1	1	1	1	1	1	1	1	1	1	1	1	1	1	1	1	1	1	1	1	1	1	1
GTG2	1	1	1	1	1	1	1	1	0	0	0	0	0	0	0	0	0	1	1	1	1	1	1	1
GTG3	1	1	0	0	0	0	0	1	1	1	0	0	0	0	0	0	0	0	0	1	1	1	1	1
GTG4	0	0	0	1	1	1	0	0	0	1	1	1	1	1	1	1	1	1	0	0	0	0	0	0

power systems. The BESS sizing problem is formulated as a stochastic unit commitment (SUC) problem. The SUC formulation is data-driven and includes three sources of uncertainty (load, wind speed and solar irradiation), battery degradation modelling, and smart load management of the flexible load.

A non-parametric distribution (data-driven) is used for the load, wind speed and solar irradiation. As, for example, the load data on offshore oil and gas platforms (OOGP) do not usually follow a normal distribution as the load in interconnected power systems does. A data-driven scenario generation and reduction approach that preserves the statistical properties of a large, generated dataset in a small number of scenarios is used. This allows reduction in the computational time and achievement of a result of high fidelity. Furthermore, a novel scenario reduction method was proposed in this work.

A case study of a real OOGP in the North Sea is considered to demonstrate the applicability of the BESS sizing method. Five test cases have been considered: Case S1 does not have BESS or flexible load, case S2 has only flexible load, case S3 has BESS with battery degradation modelled in detail and no flexible load, case S4 has flexible load and BESS without detailed battery degradation modelling and case S5 has both flexible load and BESS with battery degradation modelled in detail. All five cases are stochastic. The results obtained show that the near-optimal BESS capacities in cases S3, S4 and S5 are 35 MWh, 27.5 MWh and 27.5 MWh respectively. A 6 MW interruptible load is used in S4 and S5 which allows the reduction of the BESS capacity by 7.5 MWh. The near-optimal BESS capacities in case S3, S4 and S5 achieve 2.63 %, 2.54 % and 3.68 % cost reduction and 3.88 %, 4.43 % and 4.5 % carbon emissions reduction with respect to case S1, respectively.

Overall, this study enables multiple benefits in an isolated power system, such as enhanced security of the supply in the system, increased operational efficiency, and reduced cost and carbon emissions reduction. Moreover, the proposed, data-driven decision-making approach enables a more accurate and robust BESS sizing and the possibility of applying this study's method to other sectors such as micro-grids, remote communities and critical infrastructure. However, there are also challenges that exist with this study. Such extension, however, may come with some challenges: the complexity of the modelling and related computational tractability may be significantly affected by the size of the system under investigation. Moreover, large and high-quality datasets, which are critical for the method's application, may not be readily available in all cases. Overall, adapting the methodology in this work to sectors other than isolated power systems is possible, but may require significant effort and reworking of the method.

In the future, it will be interesting to study BESS sizing for microgrids where the DR activation has a cost. This can be another source of uncertainty which makes the problem more complex as DR activation cost will vary in real time. Future work will also look into how the operation of the BESS along with the thermal power plants from day-to-day can be optimized after the BESS has been sized and installed. Particularly for microgrids that have seasonal load profiles, it will be interesting to see how to best operate the BESS in different days and seasons.

CRediT authorship contribution statement

Ayotunde A. Adeyemo: Writing – original draft, Writing – review & editing, Visualization, Validation, Software, Methodology, Investigation, Formal analysis, Data curation, Conceptualization. **Francesco Marra:** Supervision, Resources. **Elisabetta Tedeschi:** Writing – review & editing, Supervision, Project administration, Funding acquisition.

Declaration of competing interest

The authors declare no conflict of interest.

Acknowledgements

This work was supported under the programme PETROMAKS2 of the Research Council of Norway within the project “Smart Platform” with grant number 308735.

Appendix A

Table A1
Gas turbine generator parameters.

Parameter	Symbol	Value	Unit
Natural gas and gas turbines – four identical gas turbines			
Number of gas turbines	$[-]$	4	$[-]$
Maximum gas turbine power	P_k^{max}	20.2	$[MW]$
Minimum gas turbine power	P_k^{min}	6.06	$[MW]$
Fuel consumption coefficient	a_k	−0.0156	$\left[\frac{Sm^3}{MW^2}\right]$
Fuel consumption coefficient	b_k	221.52	$\left[\frac{Sm^3}{MW}\right]$
Fuel consumption constant	c_k	1267.7	$\left[\frac{Sm^3}{hour}\right]$
Carbon emission coefficient	x_k	−0.0325	$\left[\frac{kg_{CO_2}}{MW^2}\right]$
Carbon emission coefficient	y_k	461.91	$\left[\frac{kg_{CO_2}}{MW}\right]$
Carbon emission constant	c_k	2643.4	$\left[\frac{kg_{CO_2}}{hour}\right]$
Gas turbine startup cost	u_k	440	$\left[\frac{\$}{start}\right]$
Gas turbine startup carbon emissions	d_k	1958.4	$\left[\frac{kg_{CO_2}}{start}\right]$
Minimum gas turbine up time	MUT	3	$[Hour]$
Minimum gas turbine down time	MDT	3	$[Hour]$
Ramp up limit	$ramp_k^{up}$	1200	$\left[\frac{MW}{hour}\right]$

(*continued on next page*)

Table A1 (*continued*)

Parameter	Symbol	Value	Unit
Ramp down limit	$ramp_k^{down}$	1200	$\left[\frac{MW}{hour}\right]$
CO_2 emission tax	c_{co2}	0.069	$\left[\frac{\$}{kg_{CO_2}}\right]$
Natural gas price	c_{ng}	0.4685	$\left[\frac{\$}{Sm^3}\right]$

Table A2
Battery energy storage system parameters.

Parameter values			
Battery energy storage system – Lithium iron phosphate			
Battery capacity cost	$BESS_{c\_kwh}$	500	$\left[\frac{\$}{kWh}\right]$
Battery and transformer roundtrip efficiency	$BESS_{rt\_eff}$	93	[%]
Battery HVAC load	P_{hvac}	4.5	$\left[\frac{kW}{MWh}\right]$
First cycling aging coefficient	α_{cyc_LFP}	4.42×10^{-5}	[−]
Second cycling aging coefficient	$\beta_{cyc_{LFP}}$	0.02676	[−]
First calendar aging coefficient	α_{cal_LFP}	1.985×10^{-7}	[−]
Second calendar aging coefficient	$\beta_{cal_{LFP}}$	0.051	[−]
Battery end of life	EOL	80	[%]
Battery container temperature	T_{cont}	298	[K]
Initial SOC	SOC_{ini}	61	[%]
Minimum SOC for l-th BESS	SOC_l^{min}	6	[%]
Maximum SOC for l-th BESS	SOC_l^{max}	93	[%]

Table A3
Renewable energy sources parameters.

Parameter values			
Wind farm			
Rated wind turbine power	P_w^n	8.6	[MW]
Number of wind turbines	[−]	2	[−]
Cut in speed	w_{ci}	3	$\left[\frac{m}{s}\right]$
Rated wind speed	w_n	12	$\left[\frac{m}{s}\right]$
Cut off wind speed	w_{co}	25	$\left[\frac{m}{s}\right]$
Solar farm			
Number of solar PV panels	[−]	23,007	[−]
Rated capacity of a solar PV panel	P_{pv}^n	0.00039	[MW]
Rated capacity of solar farm	[−]	8.6	[MW]
Standard solar irradiation	R_{ref}	1000	$\left[\frac{W}{m^2}\right]$
Standard temperature	T_{ref}	25	[°C]
MPPT efficiency	$MPPT_{eff}$	96	[%]
Inverter efficiency		96	[%]
Power temperature coefficient	k_{temp}	−0.29	$\left[\frac{\%}{°C}\right]$
NOCT	$NOCT$	47	[°C]

Data availability

The authors do not have permission to share data.

References

[1] S. Chapaloglou, D. Varagnolo, F. Marra, E. Tedeschi, Data-informed scenario generation for statistically stable energy storage sizing in isolated power systems, J. Energy Storage 1 (51) (2022 Jul) 104311.

[2] Y. Yang, S. Bremner, C. Menictas, M. Kay, Battery energy storage system size determination in renewable energy systems: a review, Renew. Sust. Energ. Rev. 1 (91) (2018 Aug) 109–125.

[3] R. Machlev, N. Zargari, N.R. Chowdhury, J. Belikov, Y. Levron, A review of optimal control methods for energy storage systems-energy trading, energy balancing and electric vehicles, J. Energy Storage 1 (32) (2020 Dec) 101787.

[4] https://www.iea.org/energy-system/electricity/grid-scale-storage [Accessed on 19/07/2023].

[5] M.A. Pellow, H. Ambrose, D. Mulvaney, R. Betita, S. Shaw, Research gaps in environmental life cycle assessments of lithium ion batteries for grid-scale stationary energy storage systems: end-of-life options and other issues, Sustain. Mater. Technol. 1 (23) (2020 Apr) e00120.

[6] K.B. Kwon, D. Kim, Enhanced method for considering energy storage systems as ancillary service resources in stochastic unit commitment, Energy 15 (213) (2020 Dec) 118675.

[7] Pandžić H, Dvorkin Y, Wang Y, Qiu T, Kirschen DS. Effect of time resolution on unit commitment decisions in systems with high wind penetration. In 2014 IEEE PES General Meeting| Conference & Exposition 2014 Jul 27 (pp. 1-5). IEEE.

[8] K. Bruninx, Y. Dvorkin, E. Delarue, H. Pandžić, W. D'haeseleer, D.S. Kirschen, Coupling pumped hydro energy storage with unit commitment, IEEE Transactions on Sustainable Energy. 7 (2) (2015 Dec 11) 786–796.

[9] K. Bruninx, E. Delarue, Endogenous probabilistic reserve sizing and allocation in unit commitment models: cost-effective, reliable, and fast, IEEE Trans. Power Syst. 32 (4) (2016 Oct 25) 2593–2603.

[10] U.A. Ozturk, M. Mazumdar, B.A. Norman, A solution to the stochastic unit commitment problem using chance constrained programming, IEEE Trans. Power Syst. 19 (3) (2004 Aug 2) 1589–1598.

[11] D. Bertsimas, E. Litvinov, X.A. Sun, J. Zhao, T. Zheng, Adaptive robust optimization for the security constrained unit commitment problem, IEEE Trans. Power Syst. 28 (1) (2012 Jul 24) 52–63.

[12] K. Bruninx, K. Van den Bergh, E. Delarue, D'haeseleer W., Optimization and allocation of spinning reserves in a low-carbon framework, IEEE Trans. Power Syst. 31 (2) (2015 May 15) 872–882.

[13] M. Cao, Q. Xu, J. Cai, B. Yang, Optimal sizing strategy for energy storage system considering correlated forecast uncertainties of dispatchable resources, Int. J. Electr. Power Energy Syst. 1 (108) (2019 Jun) 336–346.

[14] M.A. Mirzaei, A.S. Yazdankhah, B. Mohammadi-Ivatloo, Stochastic security-constrained operation of wind and hydrogen energy storage systems integrated with price-based demand response, Int. J. Hydrog. Energy 44 (27) (2019 May 24) 14217–14227.

[15] M. Shahbazitabar, H. Abdi, A novel priority-based stochastic unit commitment considering renewable energy sources and parking lot cooperation, Energy 15 (161) (2018 Oct) 308–324.

[16] M. Vatanpour, A.S. Yazdankhah, The impact of energy storage modeling in coordination with wind farm and thermal units on security and reliability in a stochastic unit commitment, Energy 1 (162) (2018 Nov) 476–490.

[17] K. Doubleday, J.D. Lara, B.M. Hodge, Investigation of stochastic unit commitment to enable advanced flexibility measures for high shares of solar PV, Appl. Energy 1 (321) (2022 Sep) 119337.

[18] L. Alvarado-Barrios, A.R. del Nozal, J.B. Valerino, I.G. Vera, J.L. Martínez-Ramos, Stochastic unit commitment in microgrids: influence of the load forecasting error and the availability of energy storage, Renew. Energy 1 (146) (2020 Feb) 2060–2069.

[19] M. Elkamel, A. Ahmadian, A. Diabat, Q.P. Zheng, Stochastic optimization for price-based unit commitment in renewable energy-based personal rapid transit systems in sustainable smart cities, Sustain. Cities Soc. 1 (65) (2021 Feb) 102618.

[20] V. Kumar, R. Naresh, V. Sharma, Stochastic profit-based unit commitment problem considering renewable energy sources with battery storage systems and plug-in hybrid electric vehicles, Int. J. Energy Res. 46 (12) (2022 Oct 22) 16445–16460.

[21] E. Du, N. Zhang, B.M. Hodge, Q. Wang, Z. Lu, C. Kang, B. Kroposki, Q. Xia, Operation of a high renewable penetrated power system with CSP plants: a look-ahead stochastic unit commitment model, IEEE Trans. Power Syst. 34 (1) (2018 Aug 28) 140–151.

[22] Barrios LA, Valerino JB, del Nozal AR, Escano JM, Martinez-Ramos JL, Gonzalez-Longatt F. Stochastic unit commitment in microgrids based on model predictive control. In 2018 International Conference on Smart Energy Systems and Technologies (SEST) 2018 Sep 10 (pp. 1-5). IEEE.

[23] K. Alqunun, T. Guesmi, A.F. Albaker, M.T. Alturki, Stochastic unit commitment problem, incorporating wind power and an energy storage system, Sustainability 12 (23) (2020 Dec 3) 10100.

[24] C. Wang, Z. Zhang, O. Abedinia, S.G. Farkoush, Modeling and analysis of a microgrid considering the uncertainty in renewable energy resources, energy storage systems and demand management in electrical retail market, J. Energy Storage 1 (33) (2021 Jan) 102111.

[25] J. Li, J. Zhou, B. Chen, Review of wind power scenario generation methods for optimal operation of renewable energy systems, Appl. Energy 15 (280) (2020 Dec) 115992.

[26] L. Le, J. Fang, M. Zhang, K. Zeng, X. Ai, Q. Wu, J. Wen, Data-driven stochastic unit commitment considering commercial air conditioning aggregators to provide multi-function demand response, Int. J. Electr. Power Energy Syst. 1 (129) (2021 Jul) 106790.

[27] S. Bhavsar, R. Pitchumani, M.A. Ortega-Vazquez, N. Costilla-Enriquez, A hybrid data-driven and model-based approach for computationally efficient stochastic unit commitment and economic dispatch under wind and solar uncertainty, Int. J. Electr. Power Energy Syst. 1 (151) (2023 Sep) 109144.

[28] J.L. Crespo-Vazquez, C. Carrillo, E. Diaz-Dorado, J.A. Martinez-Lorenzo, M. Noor-E-Alam, Evaluation of a data driven stochastic approach to optimize the participation of a wind and storage power plant in day-ahead and reserve markets, Energy 1 (156) (2018 Aug) 278–291.

[29] K. Pan, Y. Guan, Data-driven risk-averse stochastic self-scheduling for combined-cycle units, IEEE Trans. Industr. Inform. 13 (6) (2017 Jun 1) 3058–3069.

[30] X. Xu, Z. Yan, M. Shahidehpour, Z. Li, M. Yan, X. Kong, Data-driven risk-averse two-stage optimal stochastic scheduling of energy and reserve with correlated wind power, IEEE Transactions on Sustainable Energy. 11 (1) (2019 Jan 24) 436–447.

[31] C. Zhao, Y. Guan, Data-driven stochastic unit commitment for integrating wind generation, IEEE Trans. Power Syst. 31 (4) (2015 Sep 29) 2587–2596.

[32] T. Ding, Q. Yang, X. Liu, C. Huang, Y. Yang, M. Wang, F. Blaabjerg, Duality-free decomposition based data-driven stochastic security-constrained unit commitment, IEEE Transactions on Sustainable Energy. 10 (1) (2018 Apr 10) 82–93.

[33] H. Yang, Z. Jin, J. Wang, Y. Zhao, H. Wang, W. Xiao, Data-driven stochastic scheduling for energy integrated systems, Energies 12 (12) (2019 Jun 17) 2317.

[34] W. Xie, Y. Yi, Z. Zhou, K. Wang, Data-driven stochastic optimization for power grids scheduling under high wind penetration, Energy Systems. 14 (1) (2023 Feb) 41–65.

[35] Jordehi A. Rezaee, An improved particle swarm optimisation for unit commitment in microgrids with battery energy storage systems considering battery degradation and uncertainties, Int. J. Energy Res. 45 (1) (2021 Jan) 727–744.

[36] M. Premkumar, R. Sowmya, C. Ramakrishnan, P. Jangir, E.H. Houssein, S. Deb, N. M. Kumar, An efficient and reliable scheduling algorithm for unit commitment scheme in microgrid systems using enhanced mixed integer particle swarm optimizer considering uncertainties, Energy Rep. 1 (9) (2023 Dec) 1029–1053.

[37] Y.R. Lee, H.J. Kim, M.K. Kim, Optimal operation scheduling considering cycle aging of battery energy storage systems on stochastic unit commitments in microgrids, Energies 14 (2) (2021 Jan 17) 470.

[38] H. Alharbi, K. Bhattacharya, Stochastic optimal planning of battery energy storage systems for isolated microgrids, IEEE Transactions on Sustainable Energy. 9 (1) (2017 Jul 11) 211–227.

[39] H.O. Howlader, H. Matayoshi, T. Senjyu, Distributed generation integrated with thermal unit commitment considering demand response for energy storage optimization of smart grid, Renew. Energy 1 (99) (2016 Dec) 107–117.

[40] T. Nguyen-Duc, L. Hoang-Tuan, H. Ta-Xuan, L. Do-Van, H. Takano, A mixed-integer programming approach for unit commitment in micro-grid with incentive-based demand response and battery energy storage system, Energies 15 (19) (2022 Sep 29) 7192.

[41] M. Hamdy, M. Elshahed, D. Khalil, E.E. El-zahab, Stochastic unit commitment incorporating demand side management and optimal storage capacity, Iran. J. Sci. Technol. Trans. Electr. Eng. 1 (43) (2019 Jul) 559–571.

[42] A. Maleki, F. Pourfayaz, Optimal sizing of autonomous hybrid photovoltaic/wind/battery power system with LPSP technology by using evolutionary algorithms, Sol. Energy 1 (115) (2015 May) 471–483.

[43] H. Beltran, P. Ayuso, E. Pérez, Lifetime expectancy of Li-ion batteries used for residential solar storage, Energies 13 (3) (2020 Jan 24) 568.

[44] Pinson P, Papaefthymiou G, Klockl B, Verboomen J. Dynamic sizing of energy storage for hedging wind power forecast uncertainty. In2009 IEEE Power & Energy Society General Meeting 2009 Jul 26 (pp. 1-8). IEEE.

[45] Spinning reserve and efficiency increase data. https://github.com/ayotunde33/BESS_sizing_in_SUC_data.git.

[46] Estimating The Carbon Footprint of Utility-Scale Battery Storage. https://www.forbes.com/sites/rrapier/2020/02/16/estimating-the-carbon-footprint-of-utility-scale-battery-storage/?sh=3f6a6bd57adb [Accessed 11/01/2024].